ISTITUTO NAZIONALE DI FISICA NUCLEARE

Sezione di Genova

INFN/TC–98/10
3 Marzo 1998

P. Fabbricatore, S. Farinon:

SUMMARY OF MECHANICAL, THERMAL AND MAGNETIC ANALYSES ON CMS COLD MASS MADE AT INFN GENOVA DURING 1997

Published by ***SIS–Pubblicazioni***
Laboratori Nazionali di Frascati

INFN – Istituto Nazionale di Fisica Nucleare
Sezione di Genova

INFN/TC–98/10
3 Marzo 1998

SUMMARY OF MECHANICAL, THERMAL AND MAGNETIC ANALYSES ON CMS COLD MASS MADE AT INFN GENOVA DURING 1997

P. Fabbricatore, S. Farinon

INFN, via Dodecaneso 33, 16146 Genova, Italy

Abstract

The INFN - Sezione di Genova has been deeply involved, during last years, in the design of CMS magnet.
In order to maximise its physic performances, the evolution of that project pursued from the very beginning the goal of reaching 4 T. Many parameters, such as the conductor dimensions, the outer cylinder thickness, the type of reinforcement, etc., have been modified, from Technical Proposal[1] (December 1994) to Technical Design Report[2] (May 1997), to get the best ratio between feasibility and performances.
This note would be a sort of history of the CMS design development, by showing the effort made at Genoa to contribute to the project. In the appendixes, from A to H, all the informal report written by INFN-Genova during 1997 are collected.

1 INTRODUCTION

The basic features of CMS magnet as in Technical Proposal[1] (1994) shows a four layer winding with a 50 mm thick outer cylinder, indirectly cooled, stabilised using high purity aluminium, internally wound and full epoxy impregnated; 20000 kA was needed to produce a 4 T magnetic field. The conductor consisted of three concentric parts: the central flat Rutherford cable, the high purity aluminium stabiliser and the external aluminium alloy reinforcement. The coil was split into four longitudinal sections supported by aluminium alloy flanges.
Starting in 1994, the CMS design has been deeply investigated from the magnetic, mechanical and thermal point of view, trying to optimise its performances and feasibility. Today the most features have been fixed, even if some parameters are still under verification.

2 MAGNETIC ANALYSIS

In designing a magnet, the magnetic analysis is obviously a fundamental step, since it allows to compute the reached magnetic field and the magnetic forces that load the winding under the operating conditions.
In Appendix B the results of the 2D magnetic analysis are shown. Since the only approximation of the 2D analysis is to transform the dodecagonal structure of the iron yoke into a cylindrical one, the results, in terms of central field, stored energy, inductance and forces acting on the winding, are very accurate.
A 3D analysis is under study now, in order to evaluate the effects of the misalignments of the winding, both off-axis and angular. The model used for that analysis is shown in Fig. 1, while the preliminary results are summarised in Table I.

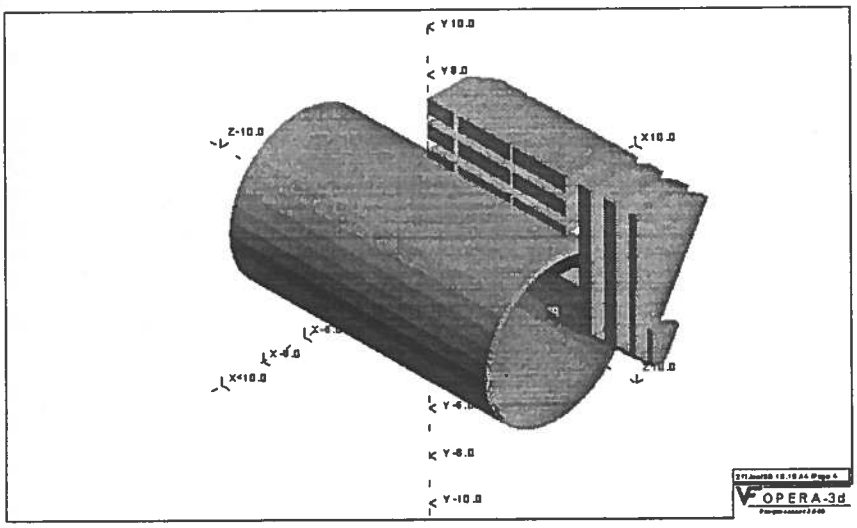

Fig. 1: 3D model of CMS magnet

Displacement	Force due to axial shift (2D model)	Force due to axial shift (3D model)	Force due to radial shift (3D model)
1 cm	85 tons	86 tons	26 tons
3 cm	254 tons	258 tons	77 tons

Table I: Preliminary results of the 3D magnetic analysis

3 MECHANICAL ANALYSIS

3.1 Introduction

In order to understand the mechanical analyses shown in Appendix A, C, D, E and H, it is necessary to explain the procedure followed to perform the mechanical computations.
Due to the complete cylindrical symmetry of the problem, only a 2D axi-symmetric section of the winding is modelled. The conductor components are modelled with its real properties: elastic and isotropic properties for the aluminium alloy, elastic and orthotropic properties for the insulation, elasto-plastic and isotropic properties, according to an experimental stress-strain curve measured at 4.2 K, for the pure aluminium. The coil has been simulated at two of its operating conditions: coil at 4.5 K, and coil at 4.5 K energised (19.5 kA, 4.05 T).

In order to obtain detailed information on the stress distribution in the winding, each conductor component must be modelled. To do so without having to produce a too large model, the choice has been made to use a submodelling approach as described below.
The stress analysis is split into two steps:

1. *Coarse model:* A preliminary stress analysis is performed using a simplified global model. Each coil component is meshed but with a limited number of nodes. Thermal and magnetic loads are sequentially applied to this model.
2. *Fine model:* A critical part of the coil is meshed. The number of elements for each component can be increased. The displacements calculated in the previous step are used as cut boundary conditions for the computations.

3.2 From Technical Proposal[1] to Technical Design Review[2]

After TP, several mechanical analyses have been made in order to understand the stress status of CMS winding, also evaluating the influence on the stress field of different conductor geometries. The conclusions were that the winding behaviour is almost the same for the different conductor configurations and that *the stress level increases by 30% in the vicinity of the Al alloy flanges.* Furthermore, in the TP design, the hoop and the axial compressive forces were supported by both a 50 mm thick Al alloy external cylinder and the reinforcement associated to the conductor.
In following developments it was argued that the modular solution involved mechanical couplings which are potential source of instability. In order to maximise the chance to get 4 T, a new concept for CMS winding was introduced. The CMS cold mass was designed to be a four layer *monolithic* 300 mm thick winding, with the mechanical structure completely associated to the conductor, instead of being partially provided by the external cylinder, making the winding a *complete self supported structure*. A thin Al alloy cylinder still surrounds the winding; it is used as cooling wall and quench back tube, but it has no mechanical function.
That was the status of CMS design at the end of 1996. Subsequent studies (see Appendix A, C and E), allowed to fix the main parameters of the conductor, geometry and dimensions, till the final draft of the TDR in May 1997.

3.3 New features

The design contained in the TDR is well recognised to be the best theoretical solution, maximising the chances to reach 4 T. Nevertheless further engineering studies pointed out the non negligible technical risks intrinsically included in the project; they are mainly associated with the production of 12 Km lengths of conductor and with the handling of a 250 tons structure as an indivisible mass.

Considering the fact that industrial experts proposed new ideas on the coupling between modules without using Al alloy flanges, the design was reverted to a modular solution, composed by five modules and four layers, internally wound and vacuum impregnated (see Appendix H).
Today the effort of the collaboration is to optimise that new design, mainly in the flange region, which is the most critical point to solve.

4 THERMAL ANALYSIS

The thermal analysis is a very useful tool to study the situations that may be critical from the point of view of the temperature rise.
Two thermal analyses have been carried out at INFN-Genova.

- As shown in §3 in the CMS winding the mechanical structure is completely associated to the conductor; that is achieved by joining Al alloy reinforcements both sides of the usual pure aluminium stabilised conductor. Appendix F contains the thermal analysis performed to understand the industrial feasibility of such conductor with Electron Beam Welding technique. The temperature gradient induced throughout the conductor by welding the Al alloy reinforcements is calculated as function of the EB speed, power and spot diameter. The main result, subsequently confirmed by experiments, is that to limit the temperature at the Rutherford cable within 180 °C, the EB speed and power should be respectively 1 m/min and 8 kW, or 2 m/min and 12 kW. No dependence on the spot diameter has been pointed out.
- In Appendix G the effect of the heat dissipation in electrical joint on the temperature distribution in the winding is analysed. Particularly the peak temperature is a very important parameter from the point of view of the stability of the magnet; it has been found to range from 4.5 K to 4.8 K, depending on the joint resistance and length. The conclusion is that 4.8 K should be taken as operative temperature.

REFERENCES

[1] CMS The Compact Muon Solenoid - Technical Proposal
CERN/LHCC 94-38, LHCC/P1, December 15, 1994
[2] CMS The Magnet Project - Technical Design Report
CERN/LHCC 97-10, CMS TDR 1, May 2, 1997

APPENDIX A

STUDY ON THE POSSIBLE USE OF HIGH STRENGTH PURE AL FOR THE CONDUCTOR OF CMS COIL

January 17, 1997

1 INTRODUCTION

In this brief paper we will present a preliminary study on the possibility to use an high strength pure aluminium for the conductor of CMS solenoid. This aluminium is pure 99.998, but contains 200 ppm Zn impurity. The mechanical strength is increased, as shown in Fig. A1, if compared with pure Al. The electrical performances are instead reduced being the RRR not higher than 500. We made our analysis looking, as first step, to the mechanical performances.

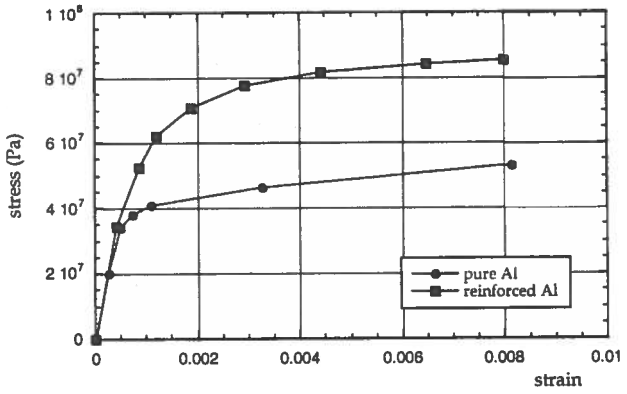

Fig. A1: Stress-strain curve for pure Al and reinforced Al

2 MECHANICAL ANALYSIS

Since we carried out the mechanical analysis of the CMS coil, we took advantage of the existing models of CMS winding for performing a Finite Element Analysis using the code ANSYS 5.2. We have mainly looked at the hoop stresses, because for a solenoid the main mechanical requirement is *to be able to support the hoop magnetic force*. The following analysis only considers the magnetic stresses.

2.1 The FEA models

In the following figures a sketch of the three models used in the mechanical FEA analysis is shown; the input models (half the magnet) have 271 turns per layer and are meshed with about 50000 nodes. The starting point of this mechanical FEA was the CMS winding present design shown in Fig. A2; the simplest approach to the problem is to replace the pure Al and the Al alloy in all the conductors with the reinforced Al (see Fig. A3).
We have also considered the possibility to have a further reinforcement by inserting Al alloy inter-layers. The overall thickness, reinforced Al conductor + Al alloy, has been maintained to 70 mm. The thickness of the Al alloy has been determined on the basis of electrical considerations. Since it is possible to assume that the RRR changes from 800 (of the pure aluminium strained at 0.15% as in the present design) to 500 (of the reinforced pure aluminium), and considering that the total resistance of the winding should be maintained constant, the result is that:

$$\frac{\rho_{800}}{A_{\text{pure Al}}} = \frac{\rho_{500}}{A_{\text{reinf. Al}}},$$

Where $A_{\text{pure Al}}$ and $A_{\text{reinf. Al}}$ are the cross sections. We find:

$$A_{\text{reinf. Al}} = \frac{8}{5} A_{\text{pure Al}} \cdot$$

It follows that the minimum reasonable value of the reinforced Al radial thickness is ~55 mm, leading to the maximum Al alloy thickness value of ~15 mm.

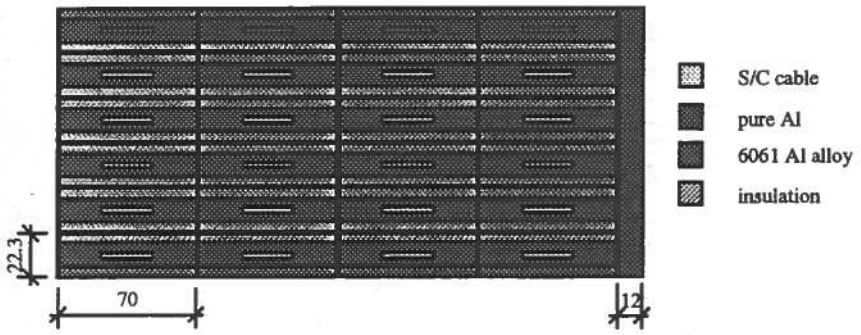

Fig. A2: CMS winding model: present design

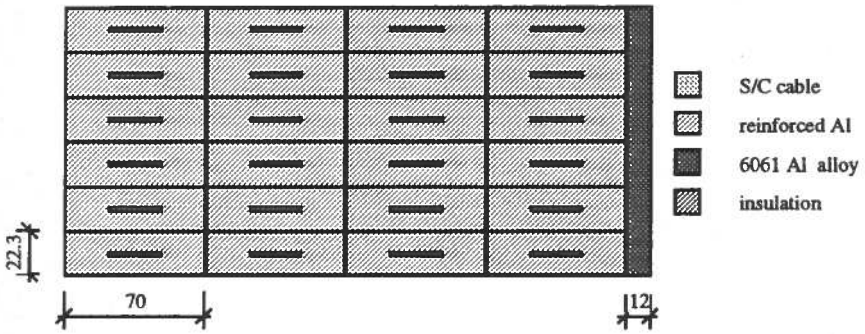

Fig. A3: CMS winding basic model using reinforced Al

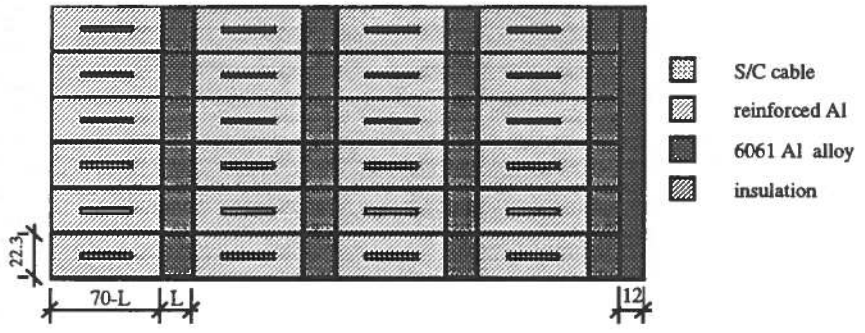

Fig. A4: CMS winding model: partial in winding-reinforcement option

2.2 FEA results

The FEA calculations have been performed for the following three options:

- basic model (no in-winding reinforcement)

- 10 mm in-winding reinforcement
- 15 mm in-winding reinforcement

at the magnetic fields of 3, 3.5 and 4 T. The results, in terms of hoop stress in the reinforced Al, are summarised in Table A.I.
In Fig. A5 the maximum hoop stress values found in the conductor are plotted as function of the magnetic field. Allowing an hoop stress as high as 53 MPa (70% of the yield), the maximum achievable field is 3.28 T. For a more conservative value i.e. 45 MPa (at the border of elastic behaviour) the maximum field is 3.0 T.

Table A.I: Hoop stress for the three considered CMS winding options

	0 mm reinforcement	**10 mm reinforcement**	**15 mm reinforcement**
3 T magnetic field	25÷45 MPa	25÷44 MPa	25÷44 MPa
3.5 T magnetic field	35÷59 MPa	35÷57 MPa	35÷56 MPa
4 T magnetic field	43÷74 MPa	43÷70 MPa	42÷68 MPa

The resulting strain is 0.11%. Higher fields can be obtained using Al alloy strips as inter-layer reinforcement. Unfortunately in order to have a reasonable benefit, working at fields above 3.5 T, the resultant hoop stress should be higher than 53 MPa, even inserting Al alloy 15 mm thick. This is due to the fact that the stress strain curves of reinforced Al and Al alloy are coincident up to 37 MPa. In the range 40 to 50 MPa there is no significant difference between the two materials.

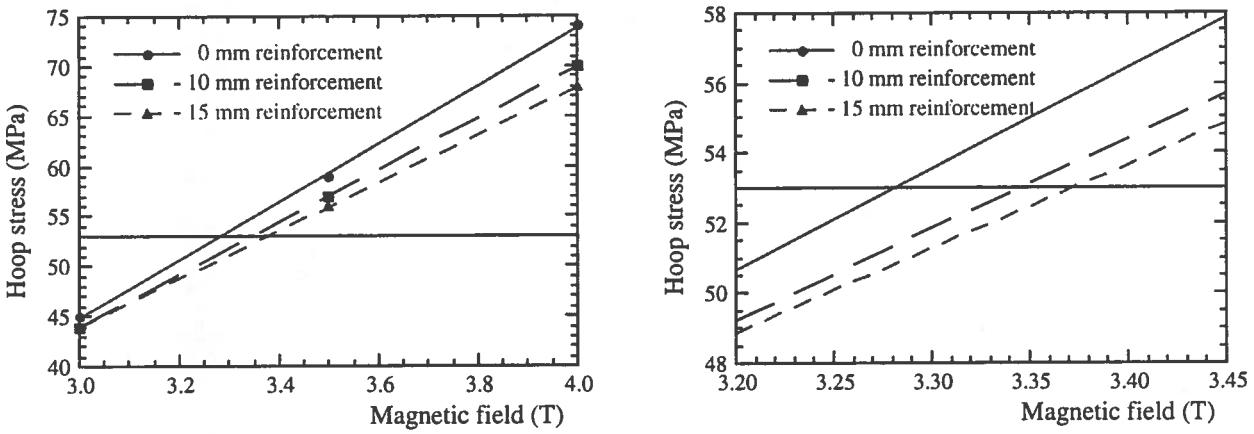

Fig. A5: Hoop stress in the reinforced Al vs. magnetic field

In Table A.II the magnetic field values corresponding to the intersection between the curves and the 53 MPa line are showed.
A maximum field of 3.38 T could be obtained using 15 mm of reinforcement. However we should consider that the cooldown to 4.5 K leads to a further increase of the stresses.

Table A.II: Magnetic field at the intersection between the curves and the 53 MPa line for the three considered CMS winding options

	0 mm reinforcement	**10 mm reinforcement**	**15 mm reinforcement**
magnetic field at the intersection	3.28 T	3.35 T	3.38 T

As conclusion we think that the high strength aluminium allows magnetic field as high as 3 T. Slightly higher fields (~ 3.25 T) can be obtained working in the plastic region of high strength aluminium. The use of Al-alloy reinforcement can increase the field of 0.1 T.

APPENDIX B

PRELIMINARY MAGNETIC ANALYSIS OF CMS MAGNET

January 27, 1997

1 INTRODUCTION

This short report contains a detailed description of all the 2D calculations performed up to now. This is obviously only a preliminary analysis: in the future complete 3D calculations (studying the tilts, the radial shifts, the presence of the chimney, and so on) will be carried out.
All the analysis was performed with the Finite Element Analysis code ANSYS; some calculations were also carried out with the FEA code OPERA 2D as comparison.

2 THE FEA MODEL

The FEA 2D model used in the magnetic calculations is shown in Fig. B1; with respect to the real magnet, having dodecagonal structure, the main magnetic analysis was carried out for the plane intersecting the dodecagon at the center of two opposite sides. A further analysis for the plane rotated of 15° (intersecting two opposite corners) was also performed and gave analogous results.
The single cables of the winding were not modeled; the four layers are thin cylinders, with 2.6 cm radial thickness, in order to reproduce the thickness of the Rutherford superconducting cable. The solenoid radius and axial length are considered at 4.5 K.
The B-H curve of the iron is shown in Fig. B2 (data from CEA).
By default the magnet is loaded with a current I_0 = 19500 A, corresponding to a current density $J_0 = 3.278 \cdot 10^7$ A/m^2.
The model is meshed with about 60000 nodes.

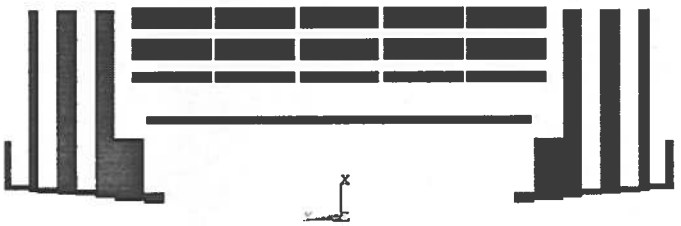

Fig. B1: FEA model for magnetic calculations

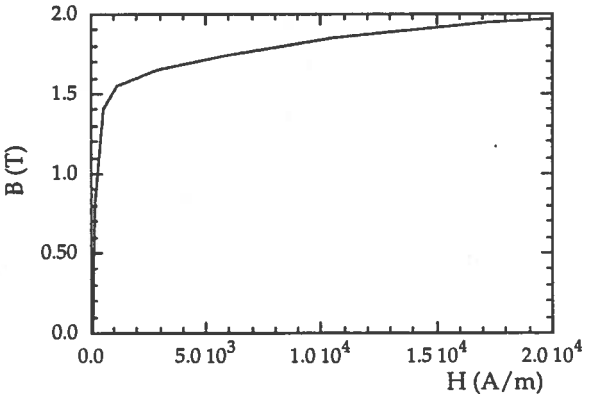

Fig. B2: B-H curve of the CMS magnet iron

3 RESULTS

The aim of the analysis was to obtain all information extractable from 2D calculations:

- the *central field*;
- the behavior of the overall flux lines and magnetic field;
- the *stored energy* and the *inductance* as function of the current and of the coil length;

- the *axial compressive force* on half the magnet and *the radial magnetic pressure* as function of the current and of the coil length;
- the *total axial force* as function of the current and of the axial shift.

In Figs. B3 and B4 the flux lines and the magnetic field corresponding to the default CMS geometry are shown; notice that there is a not negligible fringe field and that almost all the iron plates are saturated. The peak field is 4.7 T.
In Table B.I the central field values depending on the current and on the half length of the coil are shown; the field is nearly linear with the current and does not depend on slight variation of the coil length.

Table B.I: Central magnetic field

I/I_0 (%)	L/2 (m)	B_0 (T)
100	6.2	4.05
75	6.2	3.06
50	6.2	2.06
25	6.2	1.04
100	6.1	4.04
100	6.3	4.06

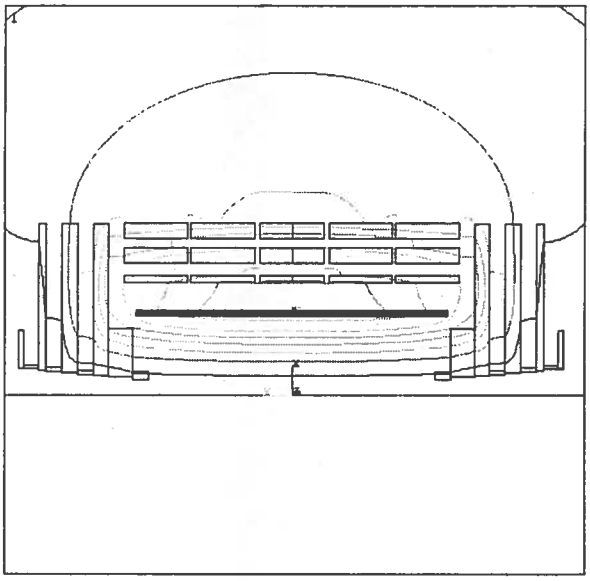

Fig. B3: Flux lines as calculated by ANSYS

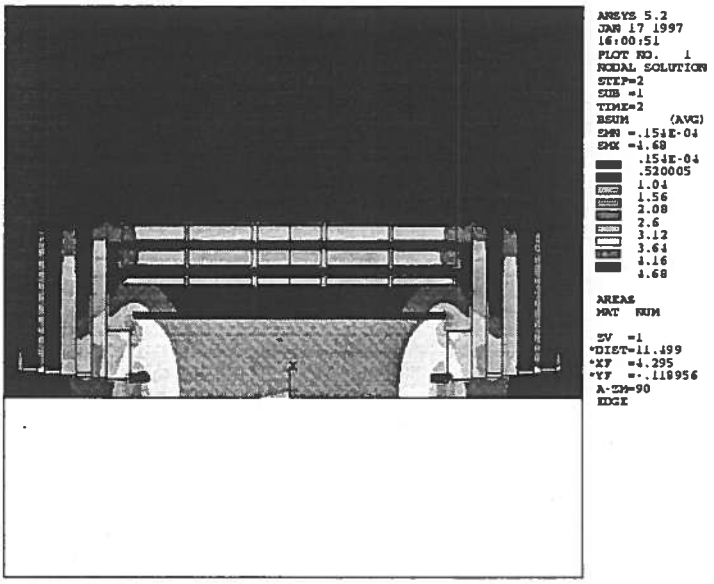

Fig. B4: Magnetic field as calculated by ANSYS

3.1 Stored energy and inductance

In Figs. B5 and B6 the stored energy and the inductance as function of I/I_0 at fixed half length of the coil (6.2 m) and as function of L/2 at fixed I/I_0 (100%) are showed.
The stored energy is calculated by integrating the vector potential on the conductors; the inductance is calculated by the stored energy using $E = \frac{1}{2} L I^2$.

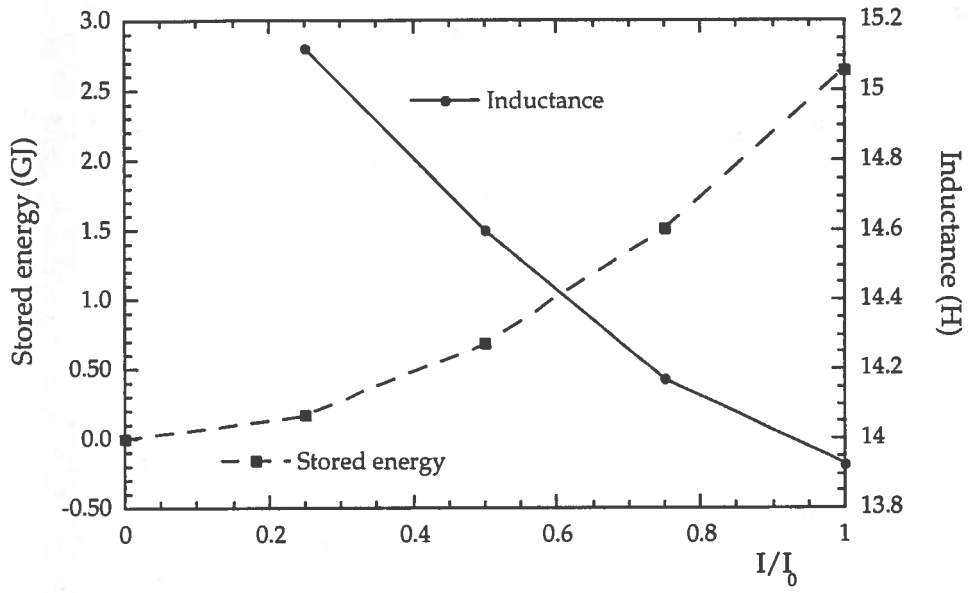

Fig. B5: Stored energy and inductance as function of I/I_0 at fixed half length of the coil (6.2 m)

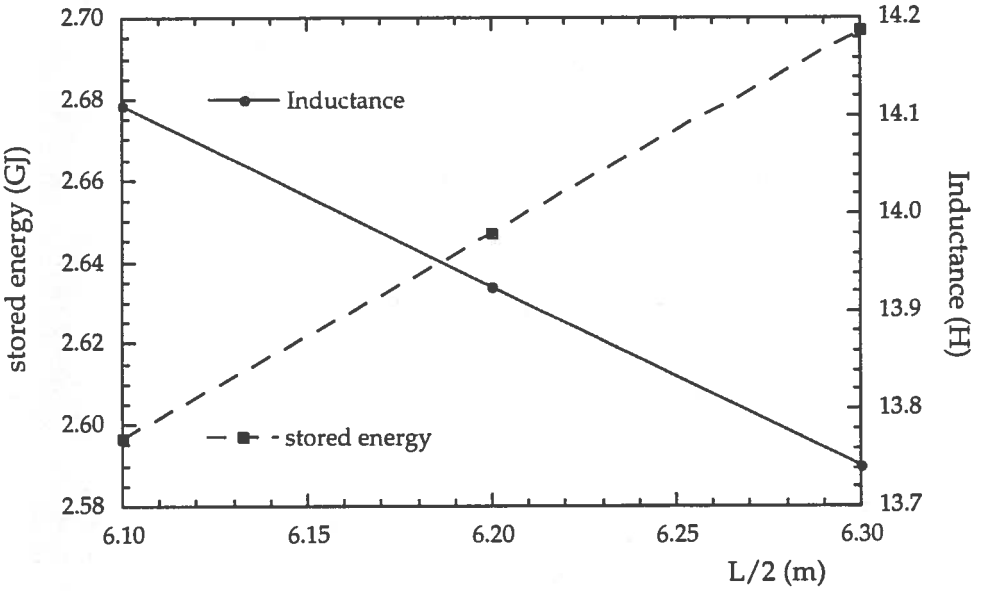

Fig. B6: Stored energy and inductance as function of the half length of the coil at fixed current (I_0)

3.2 Axial compressive force and radial magnetic pressure

In Figs. B7 and B8 the axial compressive force on the cold mass half length and the maximum radial magnetic pressure as function of I/I_0 at fixed half length of the coil (6.2 m) and as function of L/2 at fixed I/I_0 (100%) are shown.

They are calculated by integrating $\vec{J}\times\vec{B}$ on the conductors.

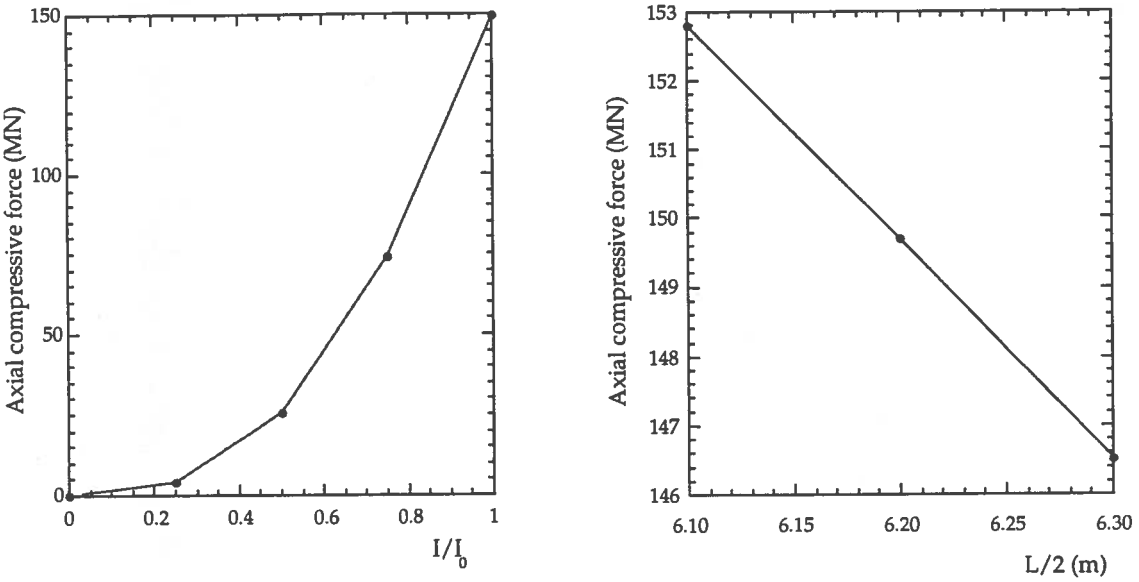

Fig. B7: Axial compressive force as function of I/I_0 at fixed half length of the coil and as function of L/2 at fixed I_0

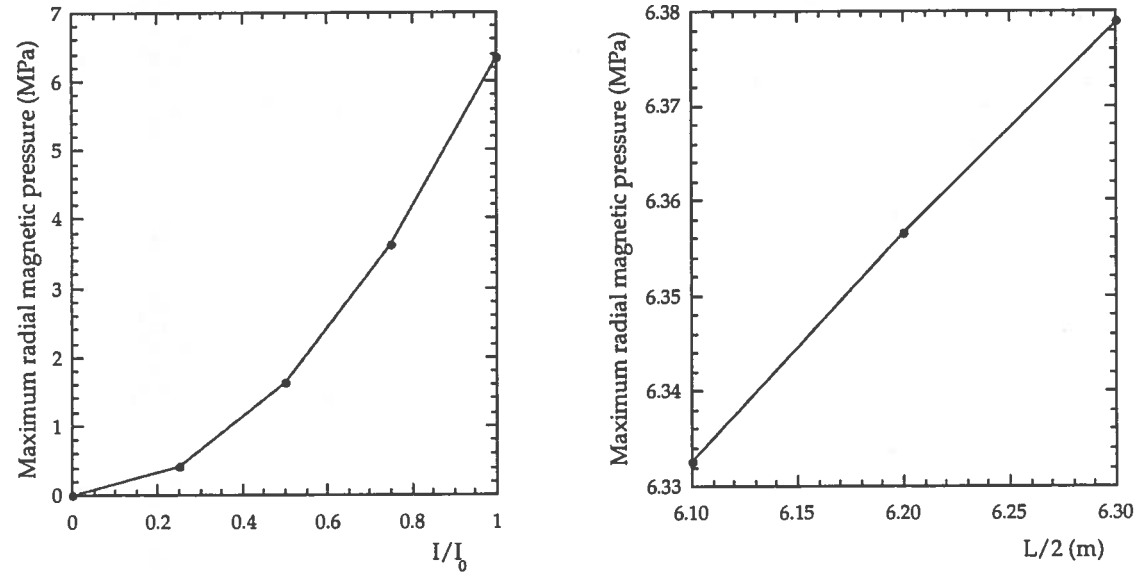

Fig. B8: Maximum radial magnetic pressure as function of I/I_0 at fixed half length of the coil and as function of L/2 at fixed I_0

3.3 Total axial force

In Figs. B9 and B10 the total axial force as function of I/I_0 at various values of the axial shift and as function of the axial shift at various values of I/I_0 is shown (in all cases L/2 = 6.2 m). The rate at 100% I/I_0 is 84 tons/cm.

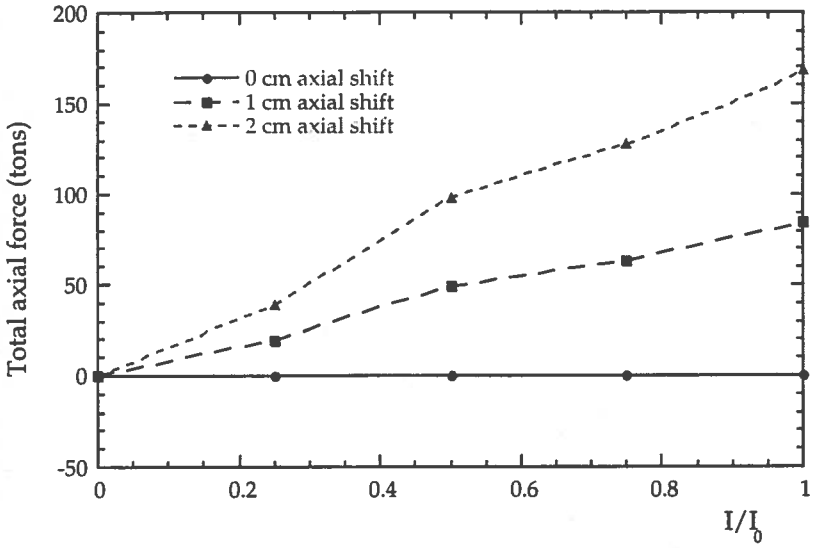

Fig. B9: Total axial force as function of I/I_0 at fixed half length of the coil (6.2 m) and at various values of the axial shift

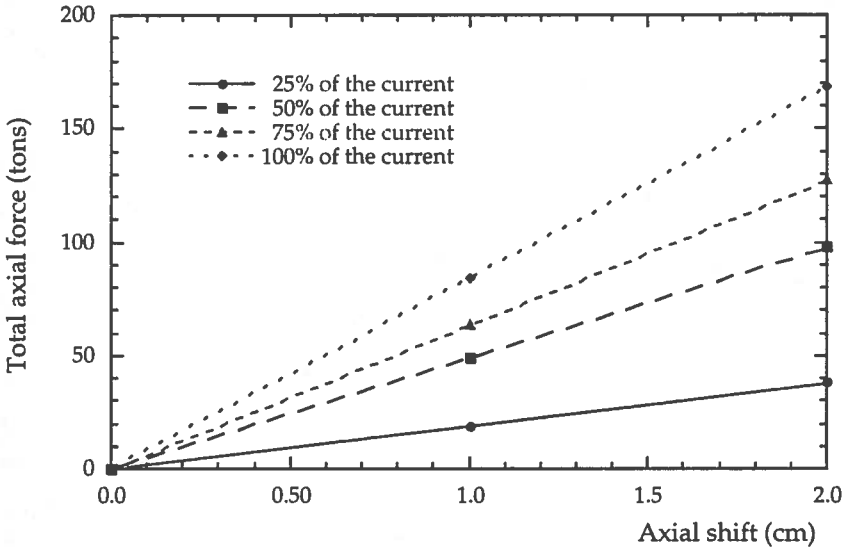

Fig. B10: Total axial force as function of the axial shift at fixed half length of the coil (6.2 m) and at various values of I/I_0

3.4 Comparison with OPERA 2D

The resulting flux lines and overall magnetic field of the default CMS geometry (I_0=19500 A, L/2=6.2 m) as calculated by OPERA 2D are shown in Figs. B11 and B12.
The peak field is 4.8 T (~2% higher than the one calculated by ANSYS); the central field is 4.05 T.

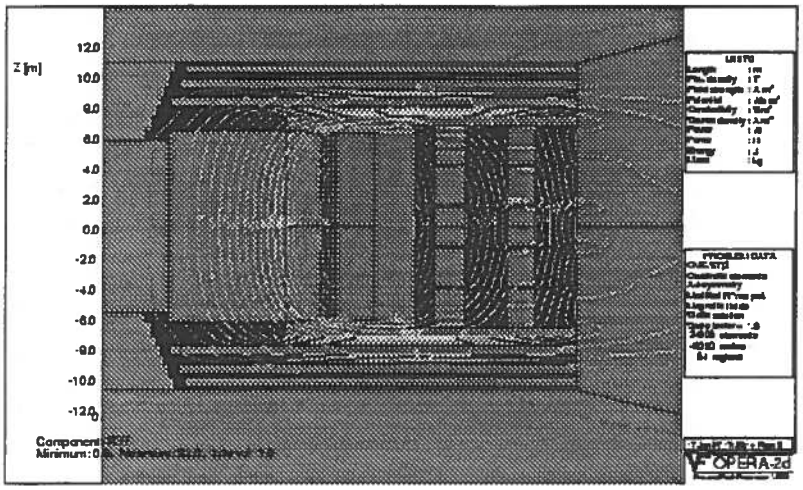

Fig. B11: Flux lines as calculated by OPERA 2D

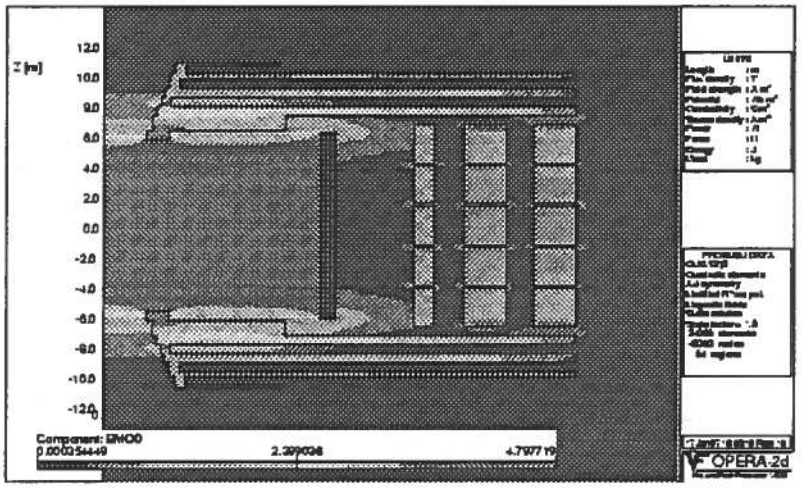

Fig. B12: Magnetic field as calculated by OPERA 2D

In Fig. B13 the stored energy and the inductance, calculated by OPERA 2D, as function of I/I_0 at fixed half length of the coil (6.2 m) are shown.

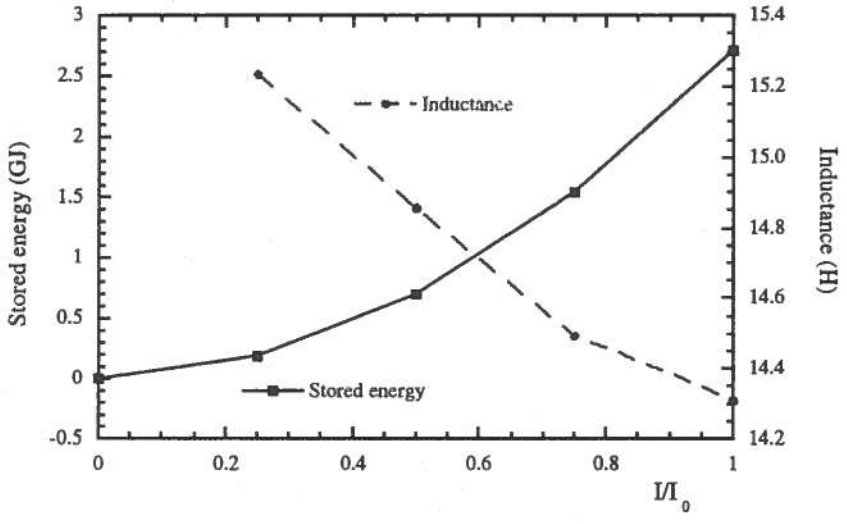

Fig. B13: Stored energy and inductance as function of I/I_0 at fixed half length of the coil (6.2 m) as calculated by OPERA 2D

APPENDIX C

REVISED MECHANICAL FEA CALCULATIONS

January 30, 1997

1 INTRODUCTION

The aim of this report is to update the mechanical calculations considering the revision of the Al insert thickness.
As usual the results are expressed in term of stress distribution in the conductor, stress distribution in the insulation and shear stress at the material interfaces; the loading conditions are the following:

- cooling down from room to operating temperature;
- superimposed magnetic forces.

2 MODEL AND MATERIAL PROPERTIES

2.1 The FEA model

The overall FEA geometry is unchanged and is shown in Fig. C1; the new conductor dimensions are show in Fig. C2.
The analysis has been carried out into the usual two steps: coarse model and fine model; the submodeled locations are shown in Fig. C1.

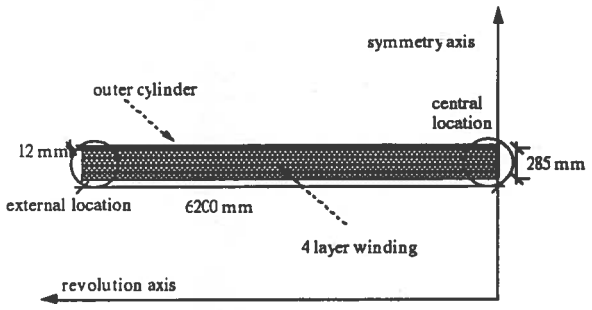

Fig. C1: Overall mechanical model

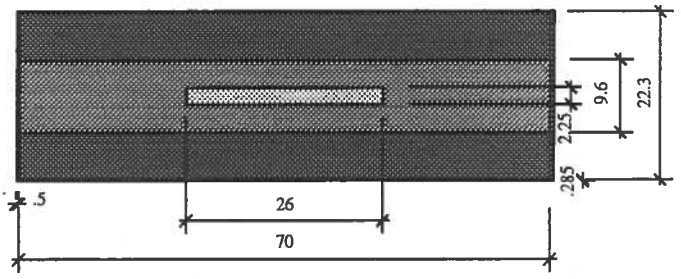

Fig. C2: Conductor geometry

2.2 Material properties

The material properties used in the calculations are the same listed in the PDR and are showed in Table C.I. The pure aluminium is considered as a plastic material.

Table C.I: Material properties used in the FEA calculations

MATERIAL	YOUNG MODULUS (GPa)	POISSON RATIO	THERMAL EXPANSION COEFFICIENT 295÷4 K (K^{-1})
Superconducting cable	130	0.3	$0.879 \cdot 10^{-5}$
Pure aluminium	78.4	0.34	$1.423 \cdot 10^{-5}$
Aluminium alloy 6061	77.7	0.327	$1.416 \cdot 10^{-5}$
Insulation parallel B	29.1 (r) 35.9 (z and a)	0.21	$2.553 \cdot 10^{-5}$ (r) $0.845 \cdot 10^{-5}$ (z and a)
Insulation perpendicular B	29.1 (z) 35.9 (r and a)	0.21	$2.553 \cdot 10^{-5}$ (z) $0.845 \cdot 10^{-5}$ (r and a)

3 RESULTS

3.1 Stress level in the insulation

The following results refer to insulation stress in the location 1 (central) and 2 (external) (see Fig. C1); the table contains the maximum and minimum values of radial, axial, hoop and principal stress. All the stresses are expressed in MPa.

Table C.II: Insulation stress in location 1 and 2; all the results are expressed in MPa

RADIAL STRESS	AXIAL STRESS	HOOP STRESS	1^{ST} PRINCIPAL STRESS	2^{ND} PRINCIPAL STRESS	3^{RD} PRINCIPAL STRESS
Thermal load – central position					
-80 → 10	-84 → 8	-85 → -69	-58 → 10	-82 → -33	-85 → -69
Thermal load – external position					
-108 → 10	-84 → 8	-85 → -61	-58 → 10	-82 → -16	-108 → -61
Thermal + magnetic loads – central position					
-88 → 8	-95 → 6	-44 → -23	-44 → 8	-62 → -24	-95 → -35
Thermal + magnetic loads – external position					
-112 → 9	-87 → 8	-62 → -35	-60 → 9	-62 → -16	-112 → -35

3.2 Overall stress in the winding

A summary of the results is given in the Tables C.III and C.IV. The maximum stress levels are shown with the indication of the location ("*" indicates all locations).

Table C.III: Overall radial, axial and hoop stress

MATERIAL	HOOP STRESS (MPa)	RADIAL STRESS (MPa)	AXIAL STRESS (Mpa)
Thermal load			
Pure Aluminum	19 [*]	33 [*]	18 [*]
SC cable	-267 [*]	-233 [*]	-13 [*]
Al alloy 6061	18 [*]	28 [*]	17 [*]
Thermal + magnetic loads			
Pure Aluminum	50 [1]	27 [*]	13 [*]
SC cable	-176 [2]	-212 [2]	-14 [*]
Al alloy 6061	119 [1]	28 [*]	16 [*]

Table C.IV: Shear stress at the bonding

MATERIAL BONDING	SHEAR STRESS (Mpa)
Thermal load	
SC cable + Pure Aluminum	21 [*]
Pure Aluminum + Al alloy 6061	20 [*]
SC cable + Insulation	19 [*]
Thermal + magnetic loads	
SC cable + Pure Aluminum	19 [*]
Pure Aluminum + Al alloy 6061	17 [*]
SC cable + Insulation	19 [*]

The strain due to the only magnetic load is 13.6%; the magnetic + thermal loads lead to a total strain of 14.3%.

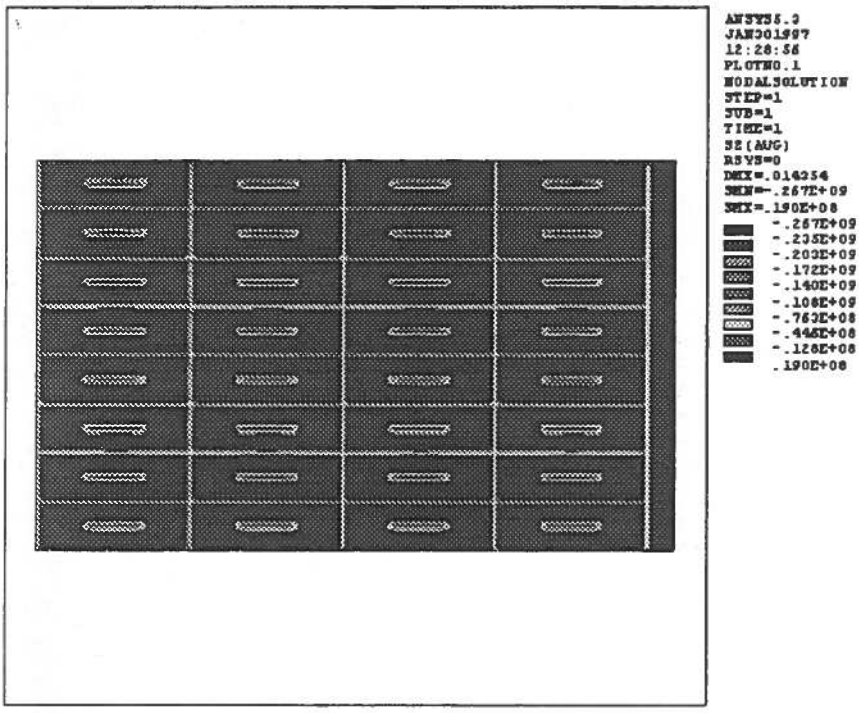

Fig. C3: Hoop stress in the central location – only thermal load

APPENDIX D

MECHANICAL ANALYSIS ON CMS WINDING

March 11, 1997

1 GENERAL CONSIDERATION

The aim of this mechanical analysis is to verify the behaviour of the CMS magnet under the action of the axial forces. This analysis has already been made, but the stress-strain curve used in calculations (saturation at 40 MPa) can be considered too much optimistic and completely not applicable to the first charge of the magnet. So new calculations with a different stress-strain curve are needed. It has been chosen an experimental curve representing pure aluminium annealed at 420 K (saturation at 10÷15 MPa). The two stress-strain curves are represented in Fig. D1.

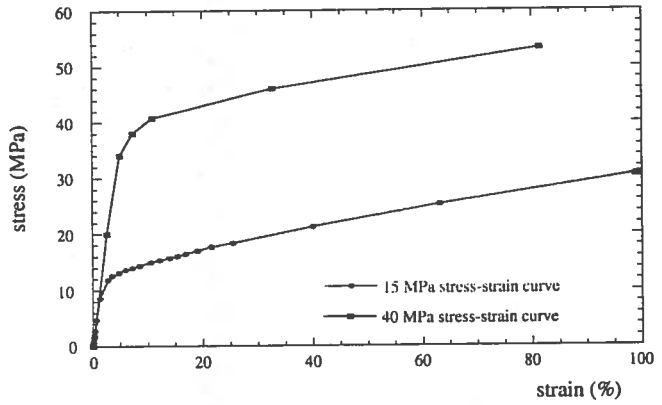

Fig. D1: 15 MPa and 40 MPa stress-strain curves

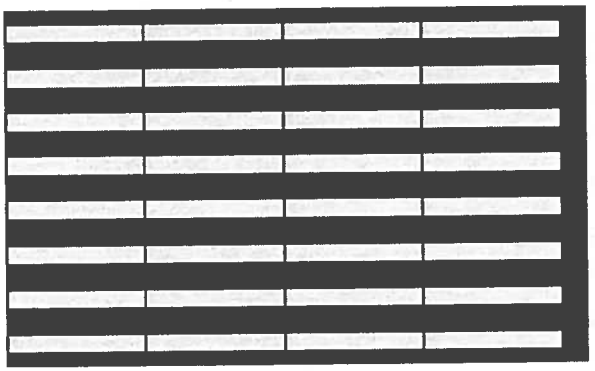

Fig. D2: Detail of the present model

To better understand the results of the analysis, the calculations will be carried out at first for the only magnetic load, applying the forces obtained by the magnetic analysis; the mechanical model represents the whole winding, without considering the effect of the Rutherford cables. In this way the analysis gives overall results; submodeling analyses should be carried out to see, for example, the details on the insulation or on the Rutherford cables.

2 PRESENT MODEL

In Fig. D2 a detail of the present model used in calculations is shown; in Table D.I some main results obtained by only energising the magnet are shown.

Table D.I: Present model results

	40 MPa stress-strain curve	15 MPa stress-strain curve
Max Von Mises stress (MPa)	41.4	16.0
Max Von Mises strain (‰)	1.94	2.35
Max Hoop strain (‰)	1.36	1.60
Max Axial strain (‰)	-0.63	-0.89

For a better understanding, in Fig. D3 the Von Mises strains (ε_{eqv}) and the axial strains (ε_y) are marked on the 15 MPa and 40 MPa stress-strain curves.
Considering the 40 MPa curve, however the equivalent strain and its corresponding Von Mises stress are very high and completely in the plastic region of the curve, the axial strain is limited and confined in the elasto-plastic region. But these results do not apply to the first charge of the magnet; considering then the 15 MPa stress-strain curve, the absolute values of the Von Mises and axial strain do not sensitively increase, but all the results are completely shifted in the plastic region.
So the first energizations of CMS magnet are very critical from the point of view of pure aluminium behaviour, since the axial resistance completely relies on the pure Al – Al alloy bonding. In this scenario, if we do not want to consider the box conductor, a possible solution is to limit the radial deformations, so that, for the Poisson coefficient effect, also the axial ones will be limited; a way to do this is the in-winding reinforcement model.

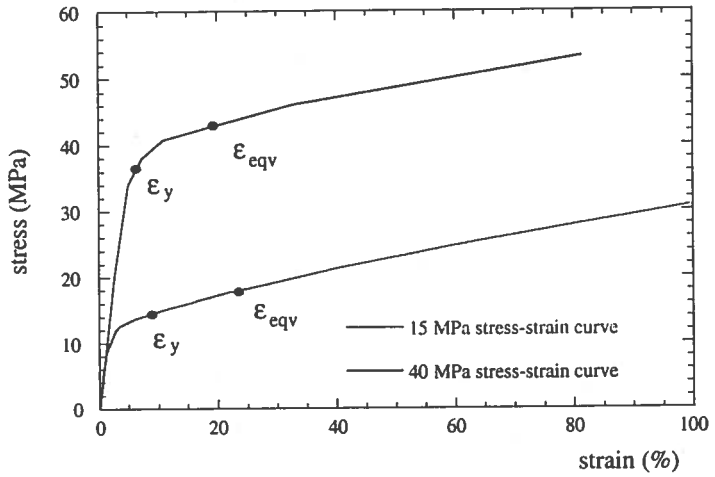

Fig. D3: Von Mises and axial strain obtained from the present model analysis

3 IN-WINDING REINFORCEMENT MODEL

In Fig. 3.1 a detail of the in-winding reinforcement model is shown; the conductors are designed so that pure Al and Al alloy materials have the same area as the present model.
The main results obtained by this analysis are shown in Table D.II and are marked on the 15 MPa and 40 MPa stress-strain curves in Fig. D4.

Table D.II: In winding reinforcement model results

	40 MPa stress-strain curve	**15 MPa stress-strain curve**
Max Von Mises stress (MPa)	41.5	16.1
Max Von Mises strain (‰)	1.97	2.43
Max Hoop strain (‰)	1.37	1.62
Max Axial strain (‰)	-0.46	-0.55

Comparing Figs. D3 and D5, it comes out that, even if the two models have about the same Von Mises stress and strain, the in-winding reinforcement model has lower values of axial strains, which is in the elasto-plastic region also during the first charge of the magnet.

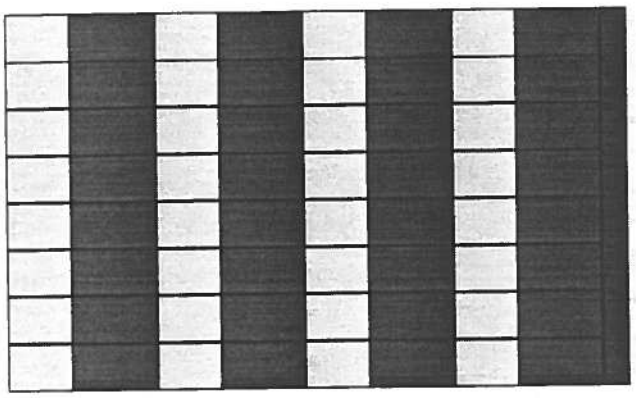

Fig. D4: Detail of the in-winding reinforcement model

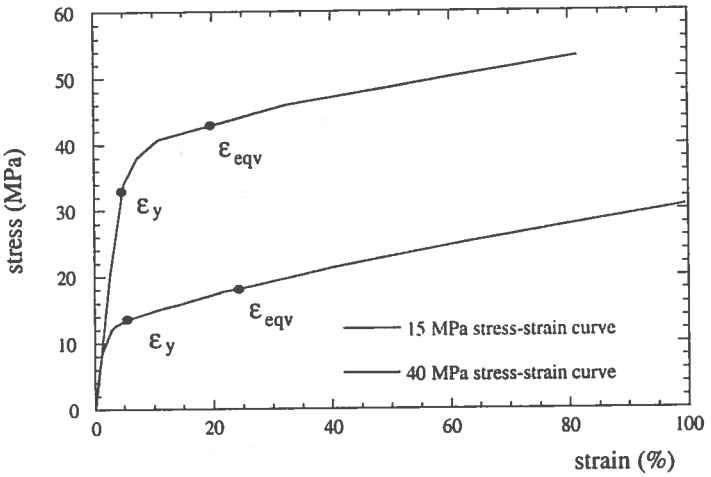

Fig. D5: Von Mises and axial strain obtained from the in-winding reinforcement model analysis

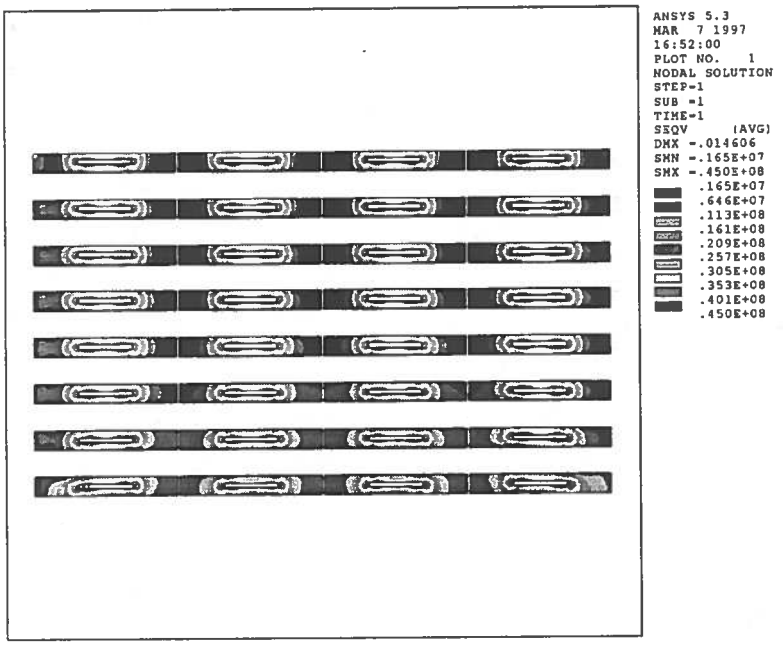

Fig. D6: Von Mises stress – only thermal load (40 MPa stress-strain curve)

APPENDIX E

IMPACT OF WINDING CONFIGURATION ON STRESSES OF CMS CONDUCTOR

April 3, 1997

1 GENERAL CONSIDERATIONS

In this report several configurations for CMS conductor will be compared in terms of the pure aluminium behaviour under the action of the axial and hoop forces.
The calculations were carried out at first for the only magnetic load, applying the forces obtained by the magnetic analysis; the mechanical model represents the whole winding, without considering the effect of the Rutherford cables. In this way the analysis gives overall results. Analysis involving sub-modelling should be carried out to obtain further information like the detailed stress distribution on the insulation or on the Rutherford cables.
Since the stress-strain for curve pure Al usually used in the past computations (yield at 40 MPa) can be considered too much optimistic and completely not applicable to the first charge of the magnet, further calculations with a more realistic stress-strain curve were needed. It has been chosen an experimental curve representing pure aluminium annealed at 420 K (yield at 10÷15 MPa). The two stress-strain curves are represented in Fig. E1.
The compared configurations are the following:

1. *New conductor configuration; left and right Al alloy reinforcement* (Fig. E2)
2. *Old conductor configuration; top and down Al alloy reinforcement* (Fig. E3)
3. *Over binding configuration* (Fig. E4)
4. *Graded over binding configuration* (Fig. E5)
5. *New conductor configuration + over binding reinforcement* (Fig. E6)
6. *Cylindrical Al alloy reinforcement configuration* (Fig. E7)
7. *Al + Zn alloy over binding configuration* (Fig. E8)
8. *Box conductor configuration* (Fig. E9)

In the figures the yellow colour represents the pure Al material, the blue colour represents Al alloy, and the green one represents the Al + Zn alloy (see Fig. E1).

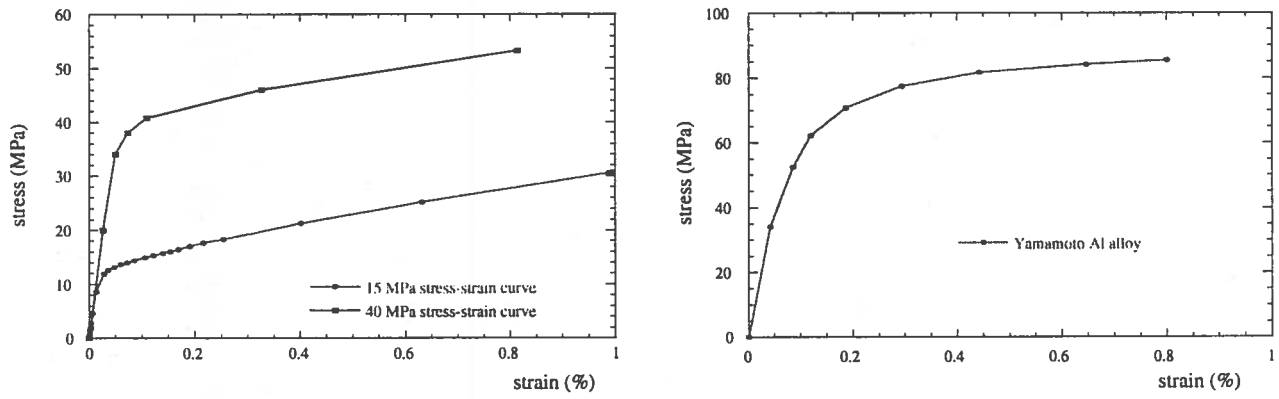

Fig. E1: 15 MPa and 40 MPa stress-strain curves (left) and Al + Zn alloy stress-strain curve (right)

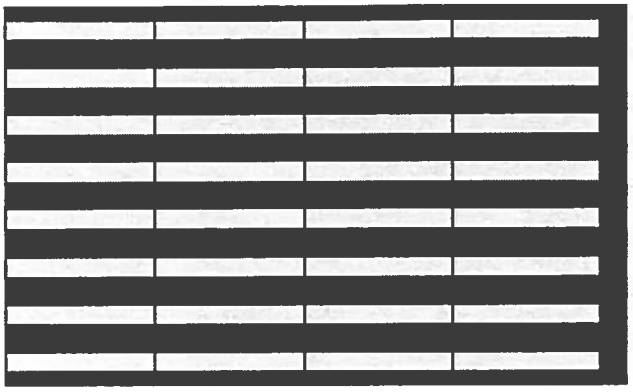

Fig. E2: Detail of the new conductor configuration

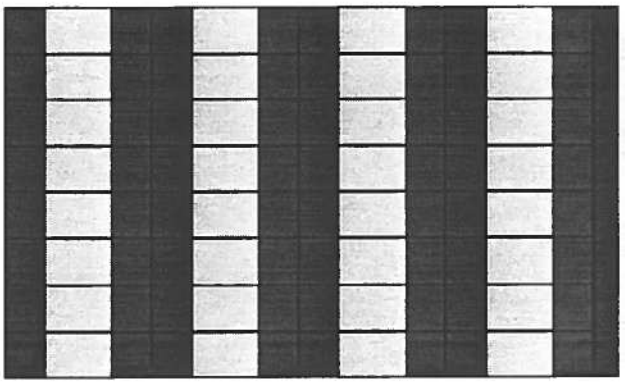

Fig. E3: Detail of the old conductor configuration

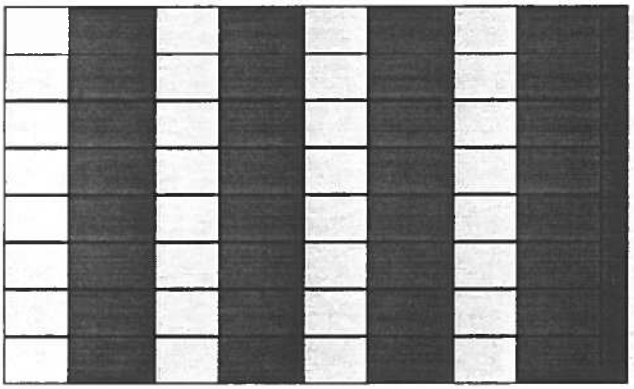

Fig. E4: Detail of the over binding configuration

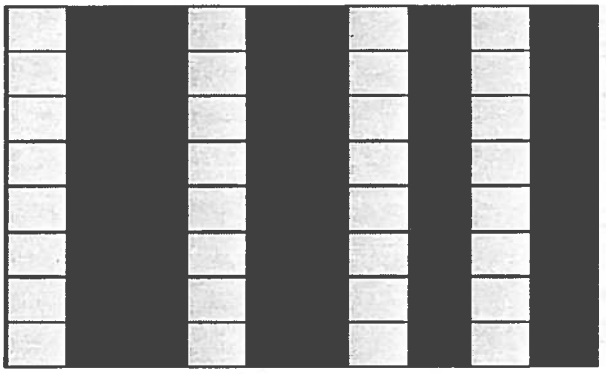

Fig. E5: Detail of the graded over binding configuration

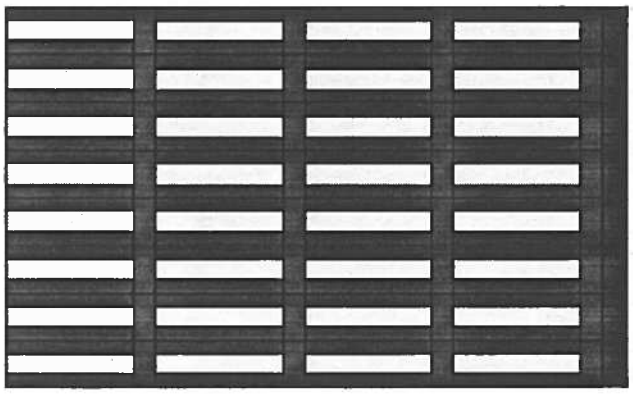

Fig. E6: Detail of the new conductor configuration + over binding reinforcement

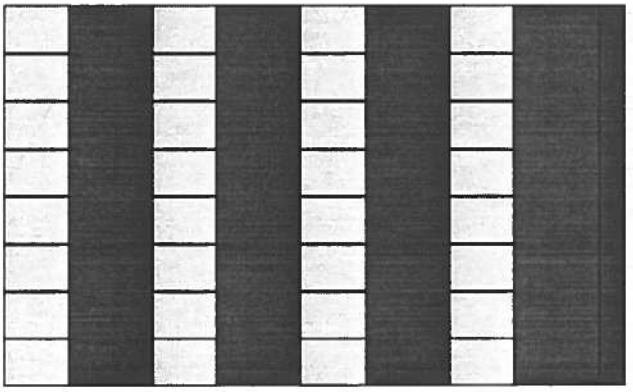

Fig. E7: Detail of the cylindrical Al alloy reinforcement configuration

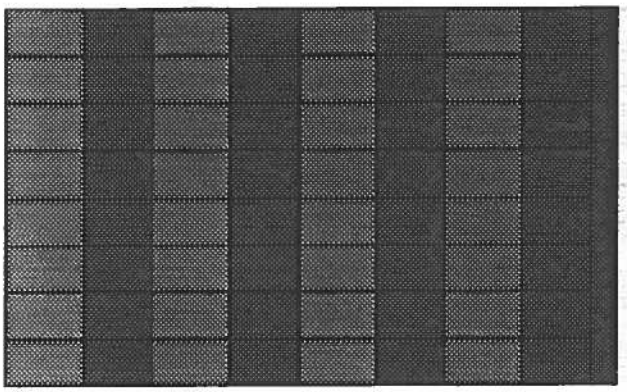

Fig. E8: Detail of the Al + Zn alloy over binding configuration

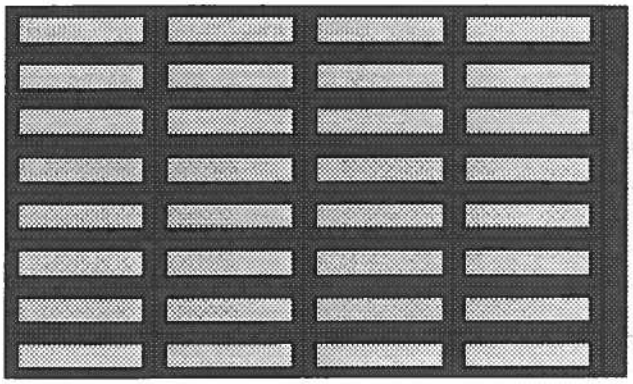

Fig. E9: Detail of the box configuration

Not all the configurations have exactly the same pure Al and Al alloy cross sectional areas; Fig. E10 the conductor geometry and dimensions are shown.
The configurations #3, #4, #6 and #7 have different geometry or material properties, but they have the same cross sectional areas.

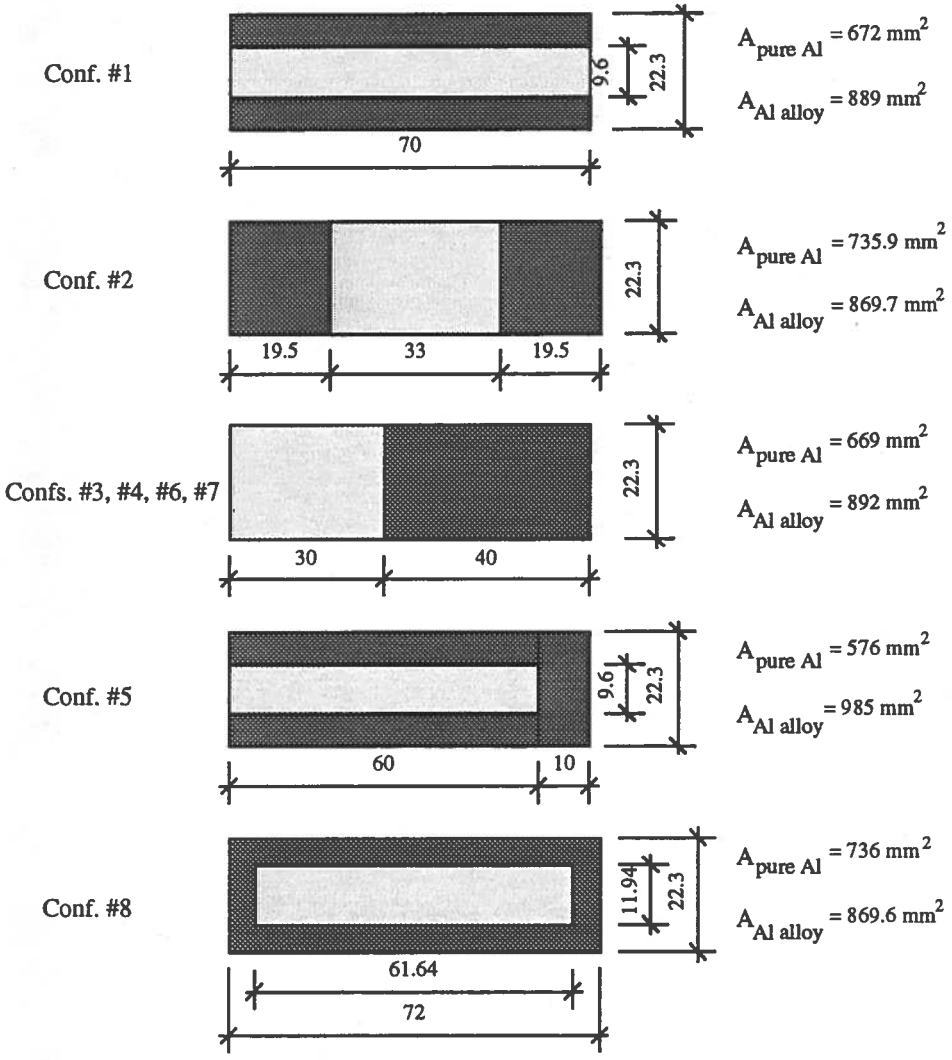

Fig. E10: Conductor cross sectional areas

2 MATERIAL PROPERTIES

In Table E.I the material properties used in computations are shown.

Table E.I: Material properties used in computations

Material	Young's modulus [GPa]	Mean integral thermal expansion coefficient [K^{-1}]	Poisson ratio
Pure Al	---	$14.23\ 10^{-6}$	0.49
Al alloy 6061	77.7	$14.16\ 10^{-6}$	0.327
SC strand	130.5	$8.79\ 10^{-6}$	0.3
Fibre glass epoxy // to solenoid's axis	35.9	$8.45\ 10^{-6}$	0.21
Fibre glass epoxy ⊥ to solenoid's axis	29.1	$25.5\ 10^{-6}$	0.21

3 OVERALL RESULTS

In Tables E.II and E.III the Von Mises stresses and strains in the pure Al and Al + Zn alloy are shown; in Table E.IV the permanent deformations, i.e. the deformations at zero stress after the magnet energization, are shown.
Considering the results obtained by the 40 MPa and 15 MPa stress-strain curves, it is clear that all the configurations are roughly equivalent from the point of view of pure Al behaviour. The only configuration #5 (new conductor configuration + over binding reinforcement) seems to be lightly better than the others, but this is because it has about 10 % more in Al alloy material.

Table E.II: Von Mises stress in pure Al and Al + Zn alloy for the considered conductor configurations

Von Mises stress (MPa)	40 MPa stress-strain curve	15 MPa stress-strain curve	Al + Zn alloy stress-strain curve
Conf. #1 (Fig. E2)	41.4	16.1	---
Conf. #2 (Fig. E3)	41.5	16.2	---
Conf. #3 (Fig. E4)	41.5	16.2	---
Conf. #4 (Fig. E5)	41.5	16.1	---
Conf. #5 (Fig. E6)	41.3	15.8	---
Conf. #6 (Fig. E7)	41.5	16.2	---
Conf. #7 (Fig. E8)	---	---	62.0
Conf. #8 (Fig. E9)	41.4	16.1	---

Table E.III: Von Mises strain in pure Al and Al + Zn alloy for the considered conductor configurations

Von Mises strain (‰)	40 MPa stress-strain curve	15 MPa stress-strain curve	Al + Zn alloy stress-strain curve
Conf. #1 (E2)	2.04	2.40	---
Conf. #2 (E3)	2.05	2.47	---
Conf. #3 (E4)	2.09	2.49	---
Conf. #4 (E5)	2.07	2.47	---
Conf. #5 (E6)	1.92	2.21	---
Conf. #6 (E7)	2.07	2.47	---
Conf. #7 (E8)	---	---	1.62
Conf. #8 (E9)	2.01	2.41	---

Table E.IV: Permanent deformation in pure Al and Al + Zn alloy for the considered conductor configurations

Permanent deformations (‰)	40 MPa stress-strain curve	15 MPa stress-strain curve	Al + Zn alloy stress-strain curve
Conf. #1 (E2)	0.8	1.3	---
Conf. #2 (E3)	0.8	1.4	---
Conf. #3 (E4)	0.8	1.4	---
Conf. #4 (E5)	0.8	1.3	---
Conf. #5 (E6)	0.7	1.2	---
Conf. #6 (E7)	0.8	1.4	---
Conf. #7 (E8)	---	---	0.4
Conf. #8 (E9)	0.8	1.3	---

Table E.V: Hoop (ε_z) and axial (ε_θ) strain in pure Al and Al + Zn alloy for the considered conductor configurations

Hoop and axial strain (‰)	40 MPa stress-strain curve		15 MPa stress-strain curve		Al + Zn alloy stress-strain curve	
	ε_z	ε_θ	ε_z	ε_θ	ε_z	ε_θ
Conf. #1 (E2)	-0.8	1.36	-0.98	1.60	---	
Conf. #2 (E3)	-0.49	1.35	-0.54	1.62	---	
Conf. #3 (E4)	-0.49	1.37	-0.56	1.62	---	
Conf. #4 (E5)	-0.48	1.37	-0.54	1.61	---	
Conf. #5 (E6)	-0.74	1.28	-0.88	1.47	---	
Conf. #6 (E7)	-0.49	1.37	-0.56	1.61	---	
Conf. #7 (E8)	---		---		-0.39	1.19
Conf. #8 (E9)	-0.76	1.34	-0.96	1.60	---	

The case of Al + Zn alloy configuration should be considered separately.
In the Appendix A has been demonstrated, with very rough electrical considerations, that the minimum reasonable value of the reinforced Al radial thickness should be ~55 mm, leading to the maximum Al alloy thickness value of ~15 mm.
In the design reported in this paper the Al + Zn alloy is 30 mm thick and the Al alloy 6061 is 40 mm thick. This leads to a result which is very good from a mechanical point of view, but which could induce weighty electrical problems, since the resistance of the winding increases up to 50%.

So, before taking into consideration the use of this design, electrical and quench back calculations should be carried out.
The conclusion is that the stress and strain on pure Al do not depend on the conductor configuration, but on the ratio of pure Al and Al alloy areas. Then it is preferable to consider a configuration in which *pure Al is not structural*, such as the old or box one (respectively #2 and #8). The best choice would be the box conductor, for which Al alloy provides completely the hoop, radial and axial strength. The less favourable configurations, but still valid, implies at least an axial continuity of Al alloy, as for confs. #2, #3 and #4. To be noted that for these configurations the axial strain is about 60% less than the others. Configurations #1 and #5 are not mechanically safe, because pure Al is completely structural. Configuration #7 (implying Al + Zn alloy) could be interesting, but quench and stability should be verified.

4 CONSIDERATIONS ON SUB-MODELLING RESULTS

Some configurations were studied more in detail using sub-modelling. Since the present design is based on reinforced conductor, results will be shown for the old (#2), box (#8) and new (#1) configurations.

4.1 Only magnetic load

The following figures show the Von Mises stress on the conductor components; they refer to the 40 MPa stress-strain curve and to the sixth conductor of the inner layer, starting from the centre of the magnet.
The deformations are 1000 times amplified.

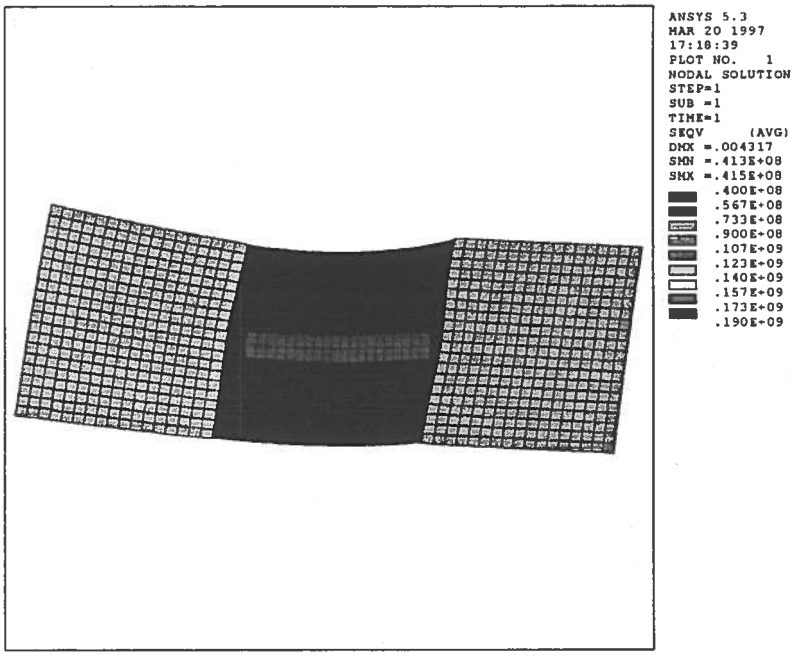

Fig. E11: Von Mises stress on the old conductor components; the deformations are 1000 times amplified (only magnetic load)

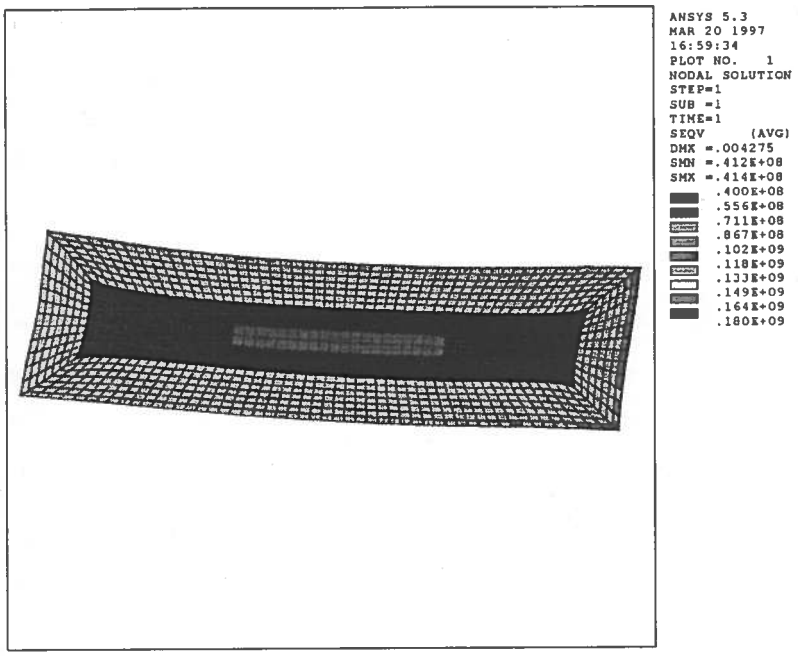

Fig. E12: Von Mises stress on the box conductor components; the deformations are 1000 times amplified (only magnetic load)

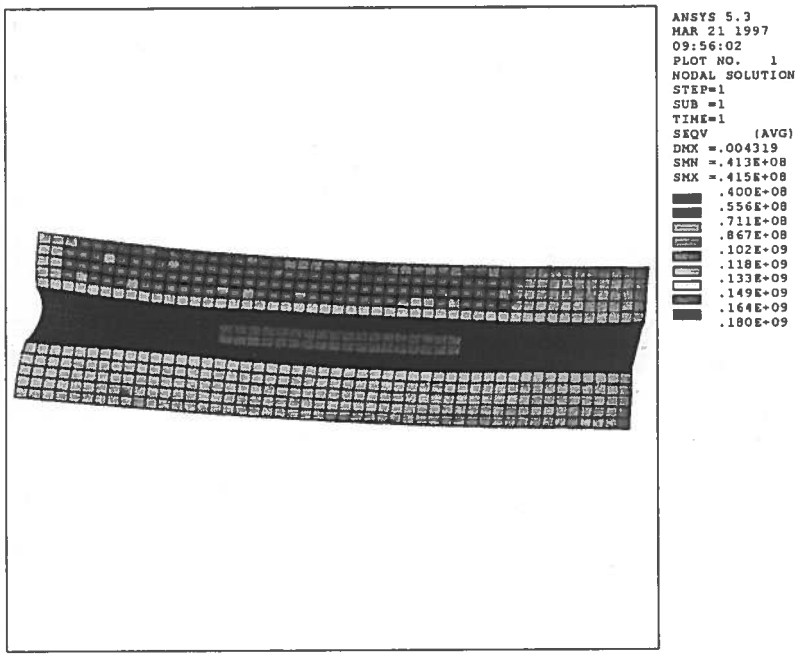

Fig. E13: Von Mises stress on the new conductor components; the deformations are 1000 times amplified (only magnetic load)

4.2 Thermal + magnetic loads

In the thermal + magnetic calculations, there is a local growth of the Von Mises stress near the Rutherford, due to the different thermal contraction between the Rutherford and pure Al. The deformed conductors show that the total effects are mainly magnetic.

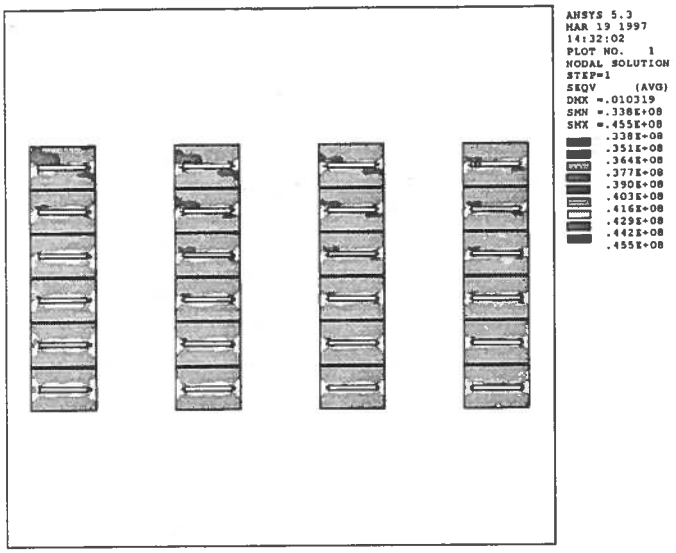

Fig. E14: Von Mises stress on the old configuration pure Al (thermal + magnetic loads)

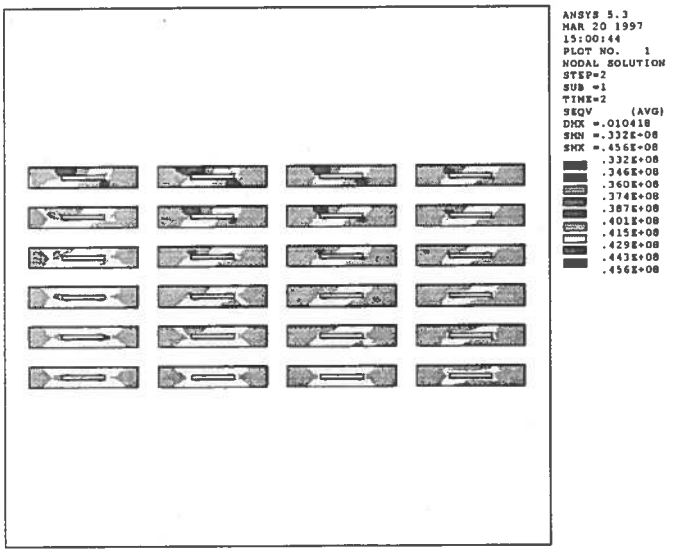

Fig. E15: Von Mises stress on the box configuration pure Al (thermal + magnetic loads)

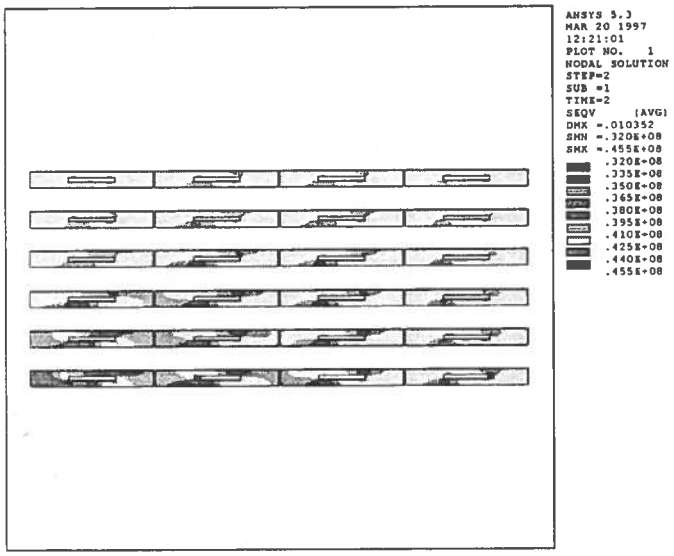

Fig. E16: Von Mises stress on the new configuration pure Al (thermal + magnetic loads)

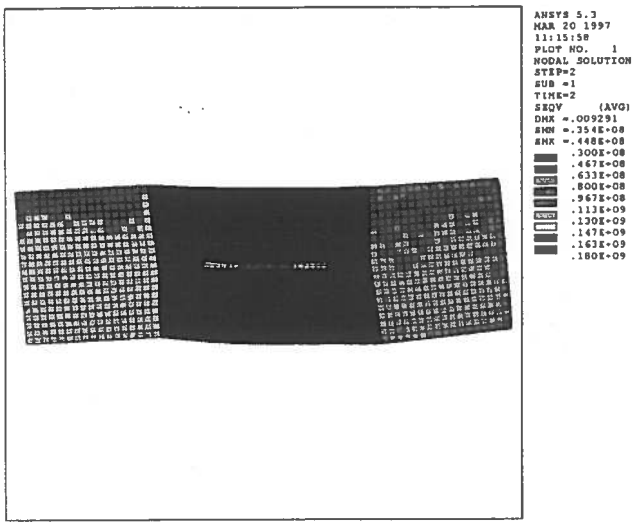

Fig. E17: Von Mises stress on the old conductor components; the deformations are 1000 times amplified (thermal + magnetic loads)

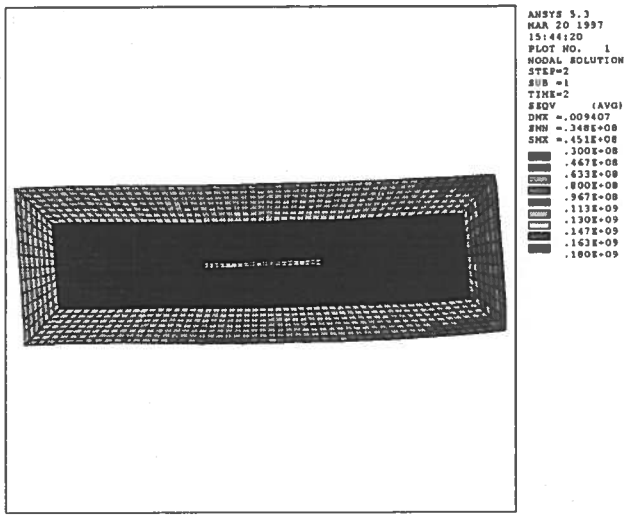

Fig. E18: Von Mises stress on the box conductor components; the deformations are 1000 times amplified (thermal + magnetic loads)

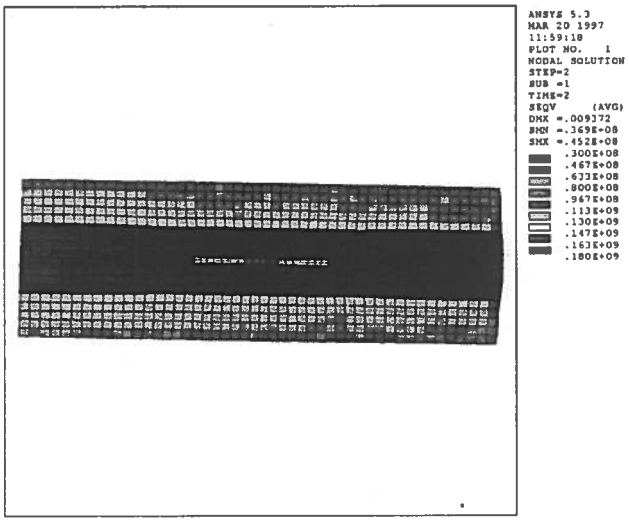

Fig. E19: Von Mises stress on the new conductor components; the deformations are 1000 times amplified (thermal + magnetic loads)

5 BLOCK CONDUCTOR

The analysis performed shows that confs. #2, #3 and #4 are possible solutions for CMS winding. For these configurations it is very important the transfer of the axial force between pure Al and Al alloy.
Though a preliminary analysis shows that the shear due to magnetic force at the pure Al - Al alloy interface is of the order of few MPa (see Fig. E20), it would be preferable to have this bonding as high as possible. This consideration leads to take as first option for the winding the block conductor.

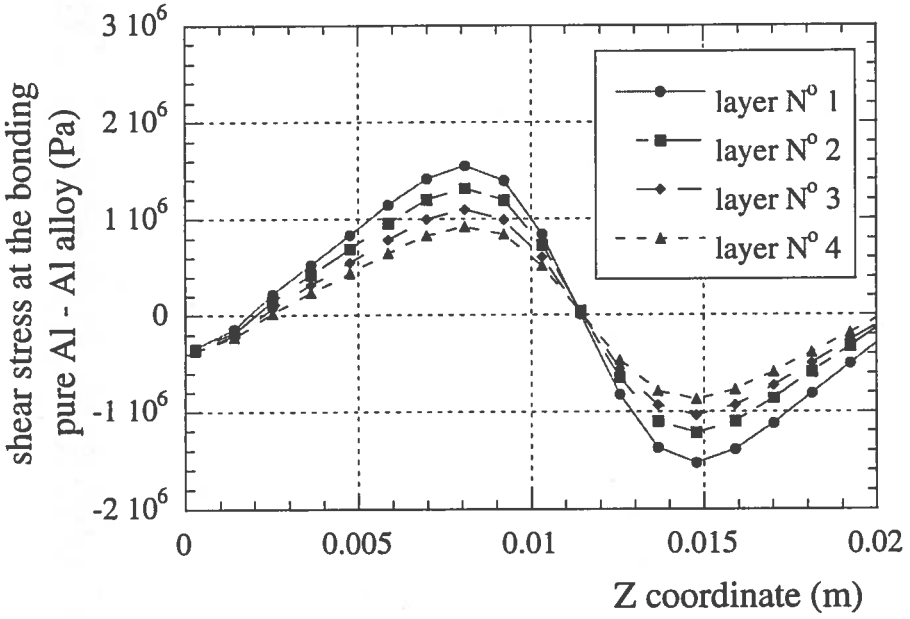

Fig. E20: Shear stress at the bonding pure Al - Al alloy for the block conductor (only magnetic load). The Z coordinate represents the magnet axes (0 m is at the centre). The layers are numbered from the inner to the outer

APPENDIX F

THERMAL ANALYSIS OF CMS CONDUCTOR DURING EB WELDING

August 1, 1997

1 GENERAL CONSIDERATIONS

The choice of joining the Al alloy reinforcement of the CMS conductor by Electron Beam Welding raises the question of the peak temperature at the Rutherford superconducting cable. In order to understand whether cable degradation can occur, we carried out a thermal analysis to study the temperature gradient induced throughout the conductor.
At the present time the block conductor, as shown in the TDR, has never been EB welded; only two samples of the ribbon conductor were welded at CERN, measuring the temperature near the Rutherford (5/6 mm from the external surface). The thermal analysis has been therefore carried on simulating first the ribbon conductor, in order to adjust the free parameters (time step, mesh size, etc.), and secondly on the block conductor, analysing the temperature profile as function of the EB speed, power and spot diameter.
Since the 3D calculations are very time consuming, a wide 2D analysis has been performed, reproducing in 3D only the most meaningful results.
For both 2D and 3D calculations, the analysis has been considered to be *adiabatic*, i.e. no heat exchange with the environment is allowed. Since it is not possible to know the temperature in the welding volume, which could be higher than the melting one, the applied load is the power provided by the EB, in form of heat generation in the welding volume.

2 THERMAL PROPERTIES

The thermal properties (specific heat, thermal conductivity, enthalpy and density) used in this analysis are considered temperature dependent. Al alloy and pure Al are considered to have the same thermal properties. The thermal properties of Rutherford cable (only for 3D calculations) are the same as copper.

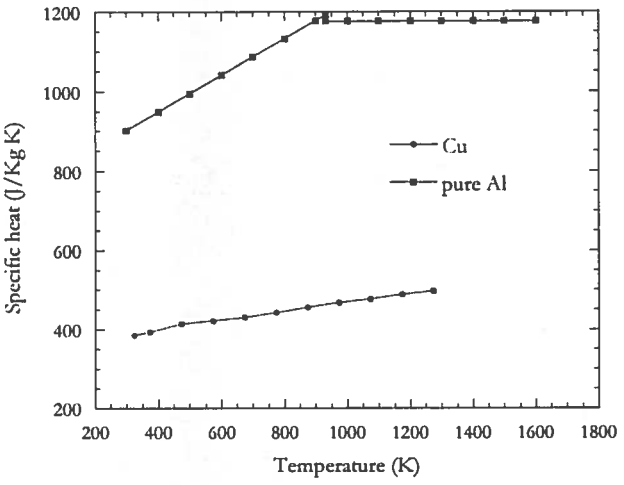

Fig. F1: Pure Al and Cu specific heat

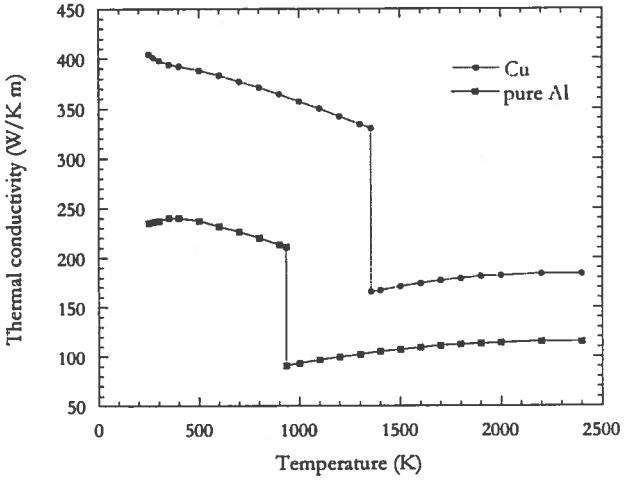

Fig. F2: Pure Al and Cu thermal conductivity

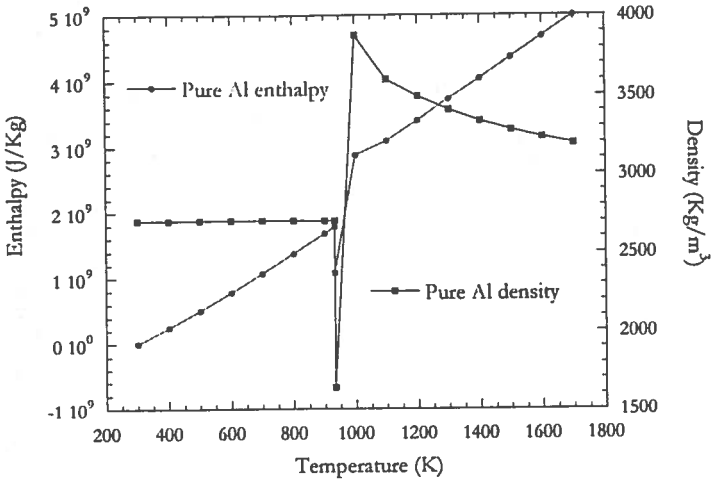

Fig. F3: Pure Al enthalpy and density

3 MESH AND TIME STEP SIZING

In a transient thermal analysis, the most crucial point is always the sizing of the mesh and the time step. In the present case those two quantities are strictly related by the speed of the EB, the critical problem becoming the discreteness of the continuos motion of the EB.
If the EB motion is supposed to be uniform, the maximum mesh size Δx and the time step Δt should follow $v = \Delta x / \Delta t$. Choosing Δx much higher than the spot diameter, and maintaining as constant the other parameters (P = 16 kW, v = 1 m/min), the results are strongly mesh dependent (see Fig. F5). The conclusion is that the maximum mesh size in the heated region should be equal to the spot diameter.

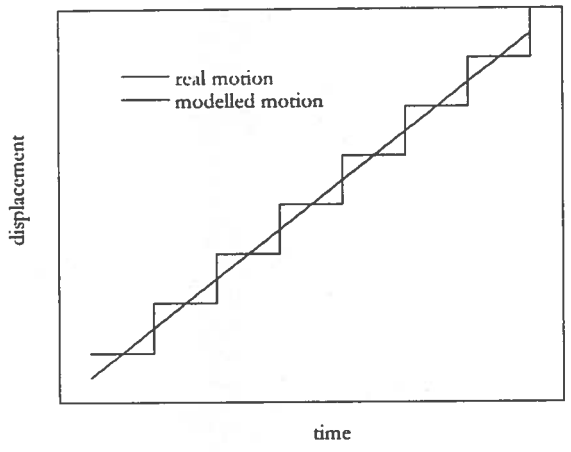

Fig. F4: EB real and modelled motion

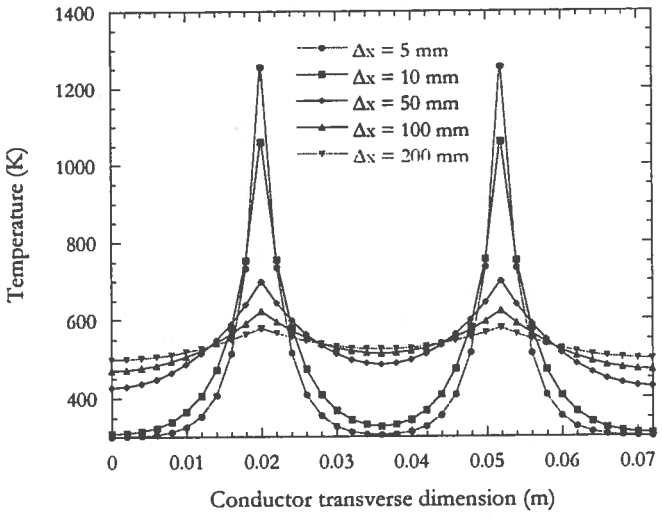

Fig. F5: Temperature profile as function of the mesh size (P=16 kW, v=1 m/min)

4 2D RESULTS

The 2D calculations are carried out on a longitudinal section of the conductors (see Figs. F6 and F10); in this way the effect of the Rutherford cable and the conduction in the transverse direction are completely neglected.

4.1 Ribbon conductor

As it was mentioned above, a sample of ribbon conductor was EB welded at CERN. The sample is shown in Fig. F6; two Al alloy coolers are placed at the sides of the conductor in order to decrease the temperature gradient near the Rutherford cable. The conductor is joined by four sequential weldings, the speed of the EB being 2 m/min. With an applied power of 16 kW, the temperature was found to be about 420 K at 5/6 mm from the Rutherford external thinner side (see Fig. F6).

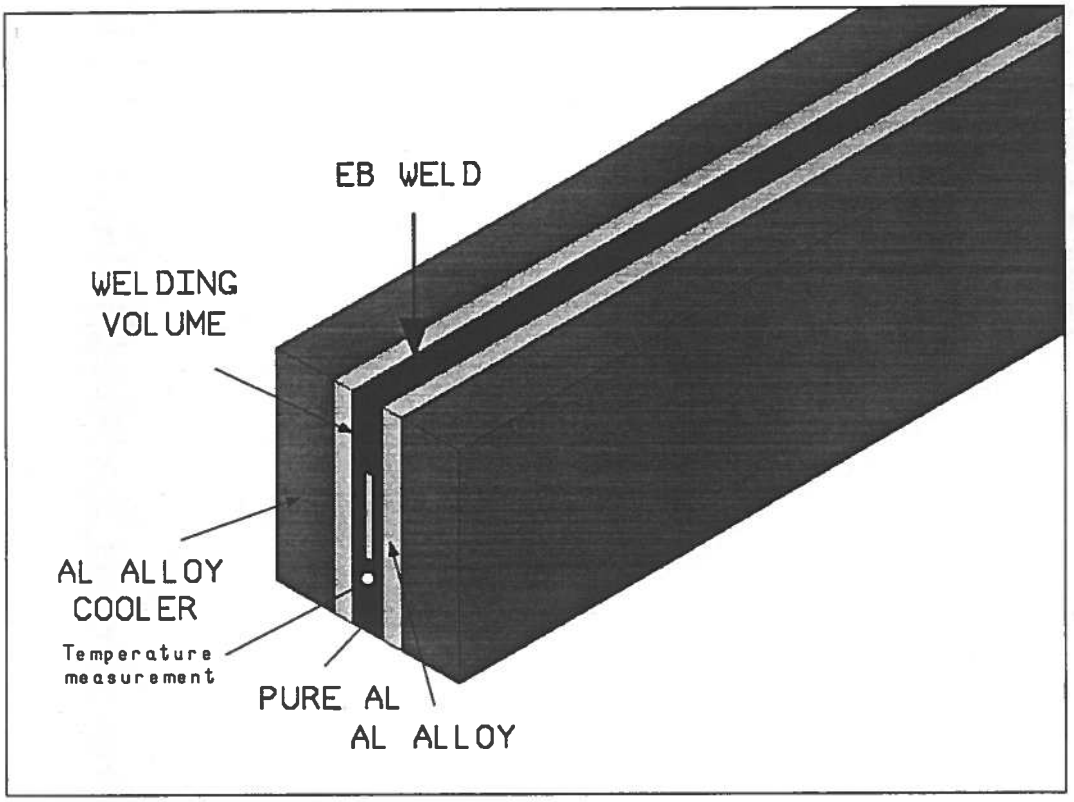

Fig. F6: Ribbon conductor

In Fig. F7 the temperature profile, as resulted from 2D calculations, is shown. The peak temperature, obviously found in the welding volume, is about 1200 K. This value should be taken as an average value, since in the direction in which it is thinner, the welding volume is meshed with only one element. This means that 1200 K, as average temperature value in the welding volume, are enough to EB weld the conductor.

To compare the FEA results with the measurement, it is necessary to consider the temperature in the Rutherford cable region (see Fig. F8), since there is an indetermination in the thermometer position. Strictly in that region the temperature is (310±30) K, but, due to the strong temperature gradient, it becomes 420 K at only 0.4 mm from the Rutherford. The conclusion is that the calculation is inside the experimental indetermination.

For comparison the same calculation has been performed at 1 m/min EB speed, maintaining as constant the other parameters. The results are shown in Figs. F9 and F10.

Also in this case, the temperature in the Rutherford cable region agrees with the measurement; this means that the grade of accuracy of the temperature measurement is not enough to distinguish the two EB speeds.

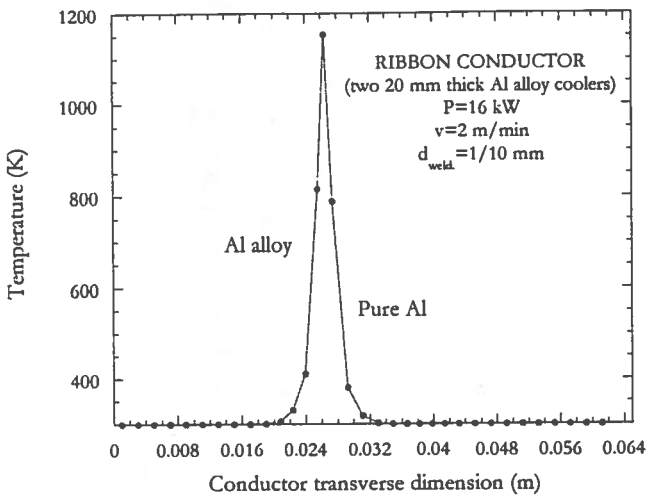

Fig. F7: Temperature profile in the cross section of the ribbon conductor (v = 2 m/min)

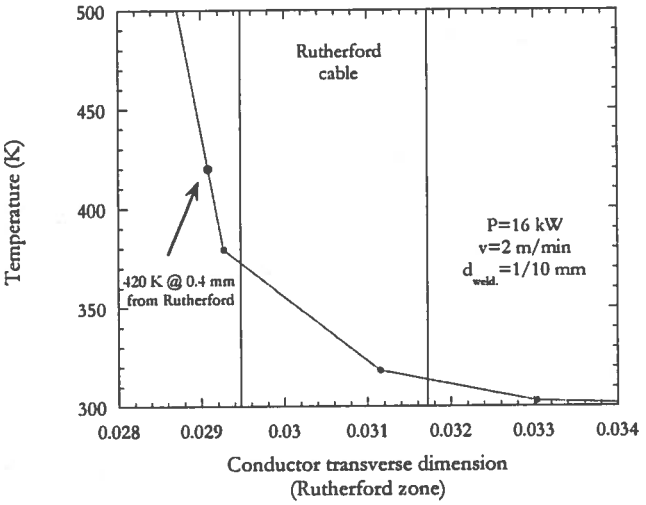

Fig. F8: Temperature profile magnification in the Rutherford cable region

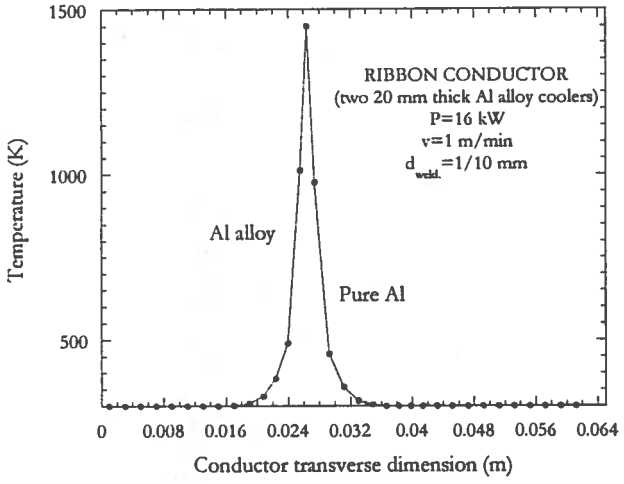

Fig. F9: Temperature profile in the cross section of the ribbon conductor (v = 1 m/min)

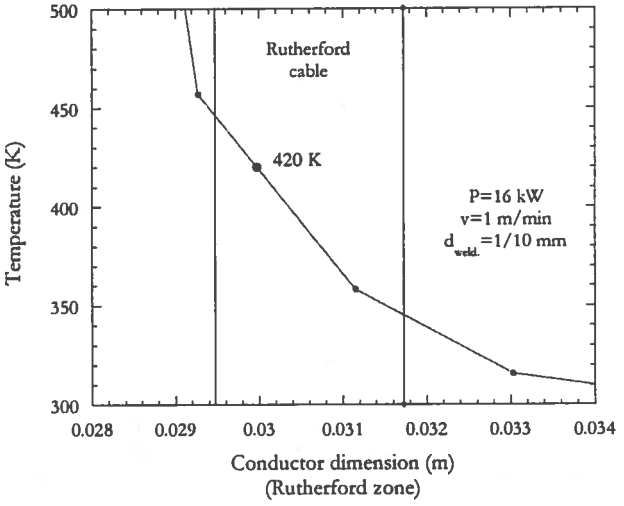

Fig. F10: Temperature profile magnification in the Rutherford cable region

4.2 Block conductor

For the block conductor, the two Al alloy reinforcements are considered welded at the same time with no Al alloy coolers (see Fig. F11). The 2D calculations are carried out on a longitudinal section of the conductors, varying the EB speed, power and spot diameter.

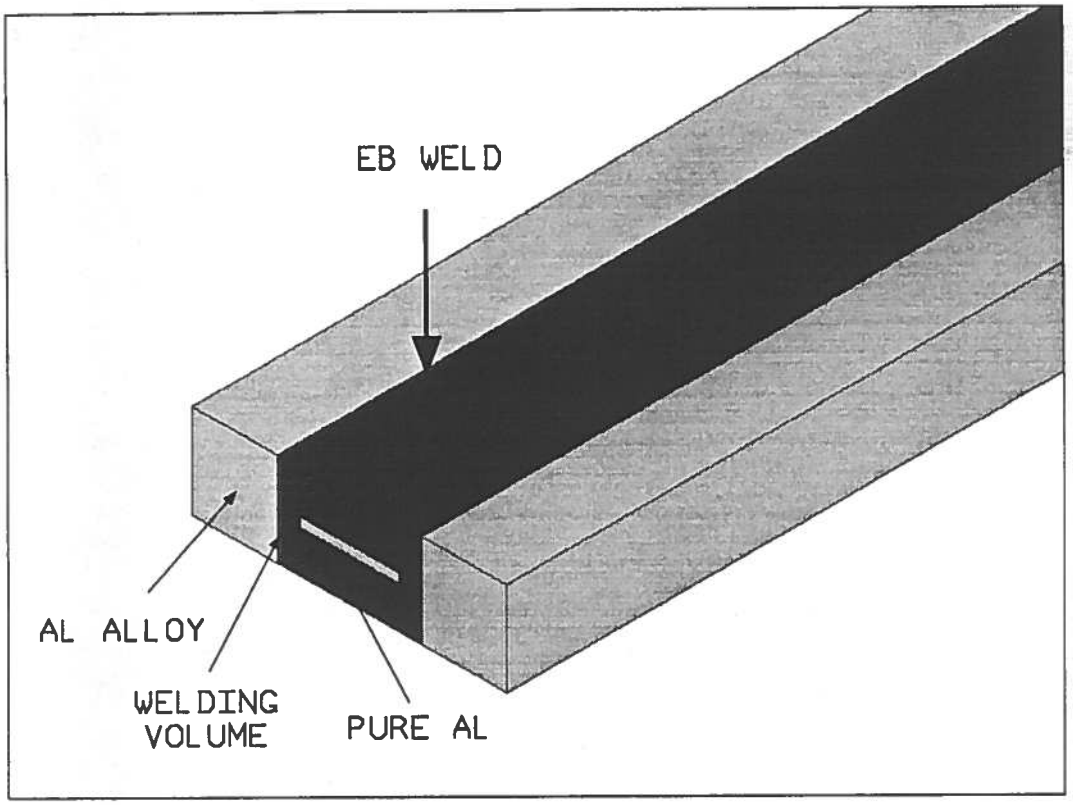

Fig. F11: Block conductor

4.2.1 Constant properties vs. properties as function of T

Some simulations have been carried out to understand the influence of the thermal properties on the temperature profiles. In Fig. F12a the overall temperature profiles obtained by properties as function of the temperature and constant properties (values at room temperature) are shown. Unfortunately these two profiles are not very different but in the Rutherford cable region (see Fig. F12b), in which the maximum temperature variation is about 80 K.
It follows that the thermal analysis, both 2D and 3D, should preferably be performed with the thermal properties as function of the temperature.

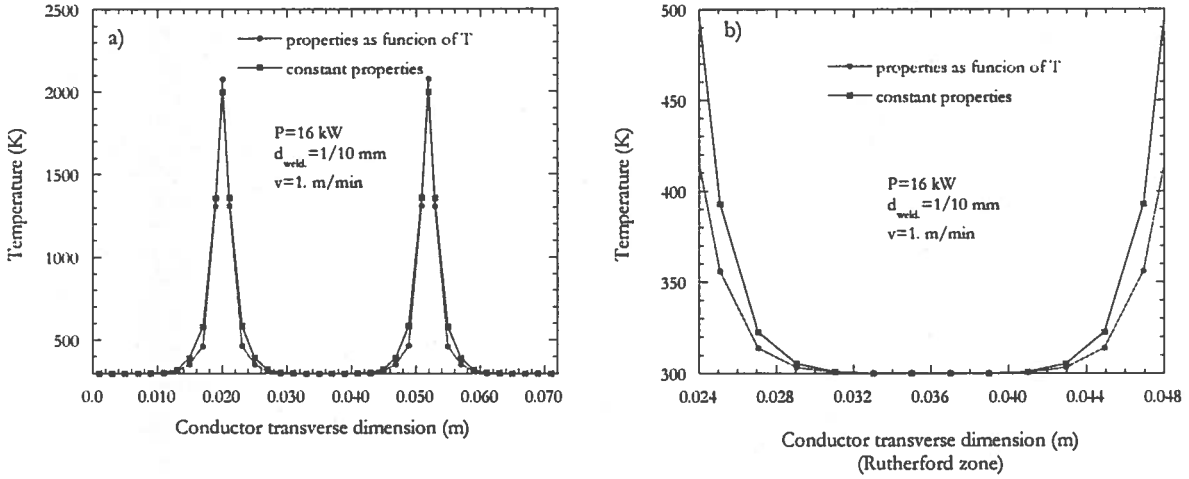

Fig. F12: Temperature profiles through the conductor (a) and in the Rutherford region (b) obtained by constant properties and properties as function of T

4.2.2 Temperature profiles as function of EB speed

In Fig. F13 the temperature profiles through the conductor (a) and in the Rutherford region (b) as function of the EB speed, at 16 kW EB power for each welding and 1/10 mm spot diameter are shown.
At that value of the applied power and for speed lower than 1 m/min, the peak temperature in the Rutherford region is not a safety value.

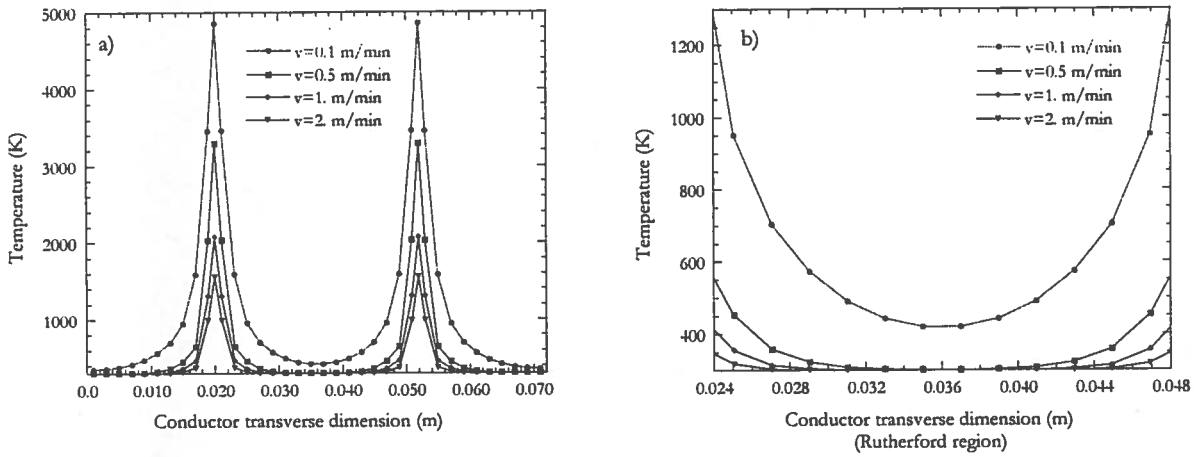

Fig. F13: Temperature profiles through the conductor (a) and in the Rutherford region (b) as function of the EB speed (P=16 kW, $d_{weld.}$=1/10 mm)

4.2.3 Temperature profiles as function of EB power

In Fig. F14 the temperature profiles as function of the EB power at 2 m/min EB speed and 1/10 mm EB spot diameter are shown. In the Rutherford cable region the three profiles are not very different, and the corresponding peak temperature is about 350 K. At the speed value of 1 m/min the peak temperature in the Rutherford region becomes about 400 K. Both the values are safe, in the sense that they can not lead to a cable degradation.

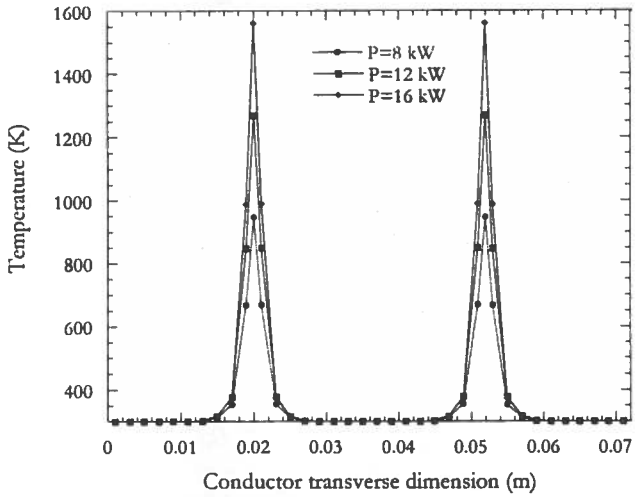

Fig. F14: Temperature profiles as function of the EB power at 2 m/min EB speed and 1/10 mm EB spot diameter

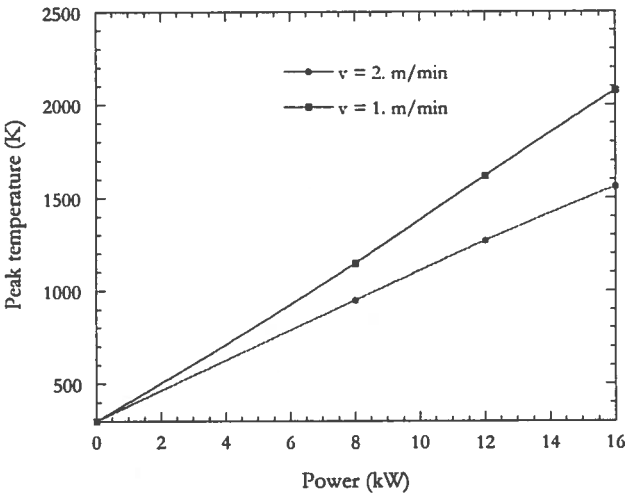

Fig. F15: Peak temperature as function of the EB power at constant EB speed and spot diameter (1/10 mm)

In Fig. F15 the overall peak temperature as function of the EB power at constant EB speed (1 m/min and 2 m/min) and spot diameter (1/10 mm) is shown. The two profiles are quite linear with the power, so that the power corresponding to a peak temperature of 1200 K, which is enough to weld the conductor (see §4.1), can be easily calculated. At the speed of 1 m/min that power is about 8 kW, and about 12 kW at the speed of 2 m/min.

4.2.4 Temperature profiles as function of EB spot diameter

The analysis shows that there is not a significant dependence of the temperature profiles on the spot diameter at least up to 5/10 mm (maintaining as constant the other parameters).

5 3D RESULTS

For completeness also a 3D calculation has been carried out; the corresponding parameters are: 16 kW EB power, 1 m/min EB speed and 1/10 mm spot diameter.
Plotting the temperature profiles across the conductor at various distances from the Rutherford cable, no differences at all were found. This means that the conduction in the cross section gives a quite negligible contribution to the temperature distribution.
In Fig. F16 the 2D and 3D temperature profiles through the conductor (a) and in the Rutherford region (b) are shown. Even if the maximum temperature in the welding volume is higher in the 3D calculation than in the 2D one, in the Rutherford region the situation is the opposite: the 2D calculation gives a peak temperature about 15 K higher than the 3D. It follows that near the Rutherford the 2D calculations are conservative.

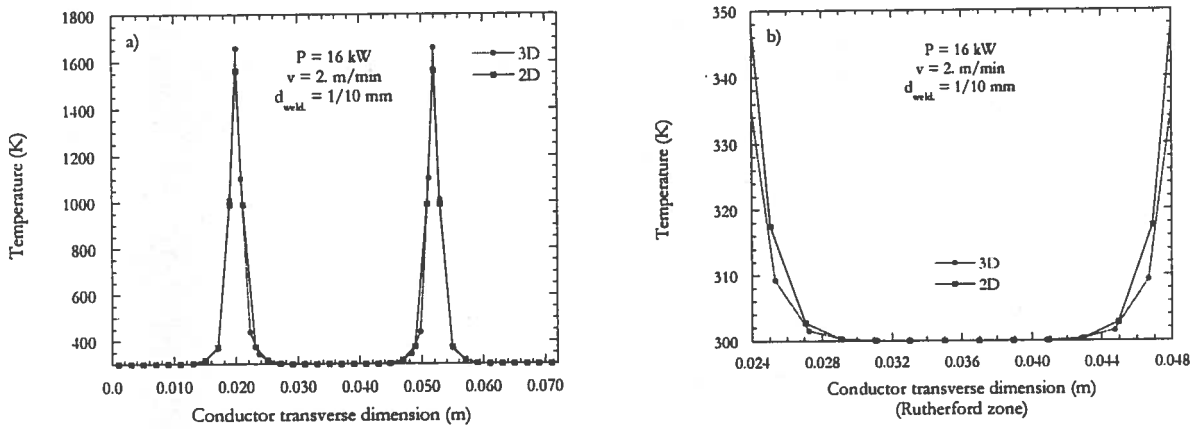

Fig. F16: 2D and 3D temperature profiles through the conductor (a) and in the Rutherford region (b)

6 CONCLUSION

The analysis has been carried out trying to simulate as close to reality as possible the behaviour of the conductor during the EB welding operation. The method of analysis was tested simulating the EB welding of the ribbon conductor.
The main results of this study are:

- The temperature profiles depend on the EB power and speed. They are less sensitive to the spot diameter (at least up to the dimension of 5/10 mm).
- In order to limit the temperature at the Rutherford within 450 K (≈180 °C), the speed must be of the order of 1 m/min with a power of about 8 kW, or 2 m/min with 12 kW.

APPENDIX G

EFFECT OF THE HEAT DISSIPATION IN CONDUCTOR JOINTS ON THE TEMPERATURE DISTRIBUTION IN THE COIL

September 9, 1997

1 GENERAL CONSIDERATIONS

The aim of this analysis is to study the peak temperature and the temperature distribution in the CMS winding due to a joint transition.
The finite element model is shown in Fig. G1; it contains the four layers and the outer cylinder and it is long as half the magnet.

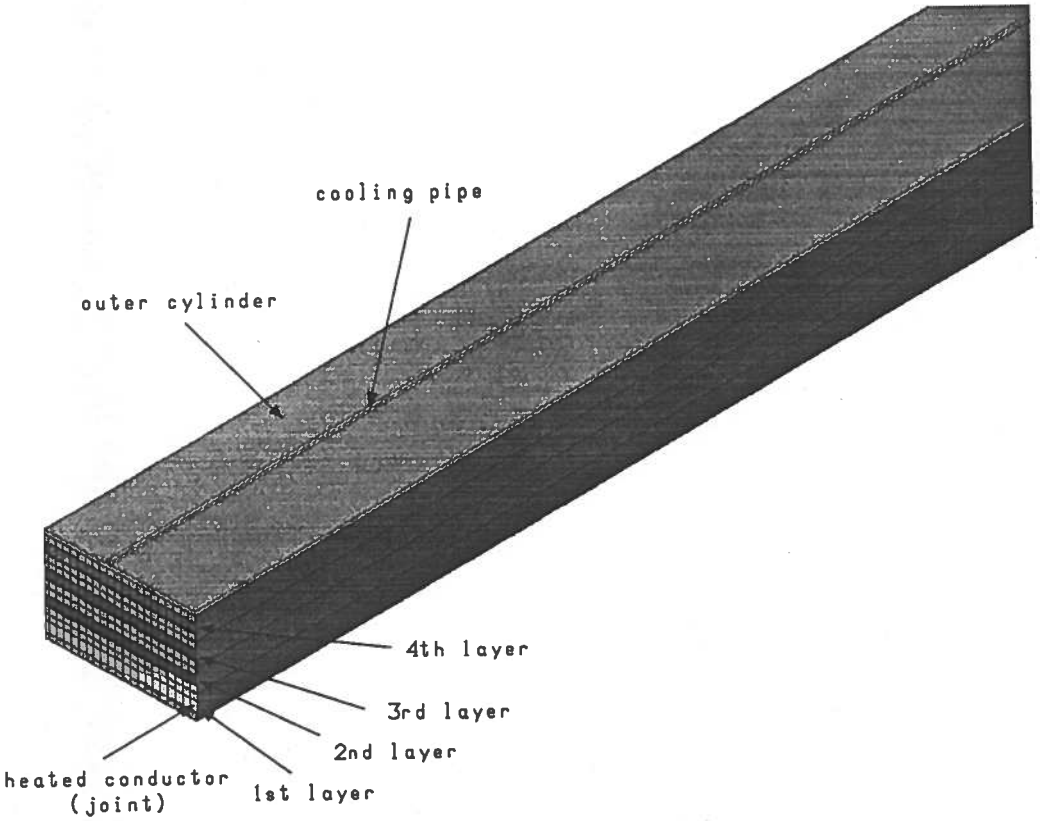

Fig. G1: Finite element model

The joint is simulated by imposing a uniform dissipation on a fixed length of conductor, the heated conductor is in the inner layer (see Fig. G1).
The assumptions are the following:

- the winding radius is supposed to be infinite (straight model);
- only the nearest cooler has been modeled, neglecting the second order effects;
- no radiation effect has been taken into account;
- the effects of the Rutherford cable are neglected;
- the thermal properties are considered not temperature dependent in the range 4÷5 K (see §2).

2 THERMAL PROPERTIES

The only material property that is needed for static thermal computations is the thermal conductivity:

- thermal conductivity of Aluminum alloy: $10.7\ {}^{W}/_{m \cdot K}$
- thermal conductivity of insulation: $0.064\ {}^{W}/_{m \cdot K}$
- thermal conductivity of pure Aluminum in the conductors (RRR=800):

B (T)	$k\ \left({}^{W}/_{m \cdot K}\right)$
1	2210
2	1810
3	1690
4	1640

3 RESULTS

The parameters taken into account are:

- the joint resistance ($1 \cdot 10^{-9}$, $2 \cdot 10^{-9}$ and $5 \cdot 10^{-9}$ Ω);
- the joint length (0.5 and 1. m);
- the distance between coolers (0.1, 0.2, 0.3 and 0.4 m).

In Figs. G2 and G3 the peak temperature as function of the joint resistance for various values of the distance between coolers and corresponding to a joint length of respectively 1 m and 0.5 m is shown.

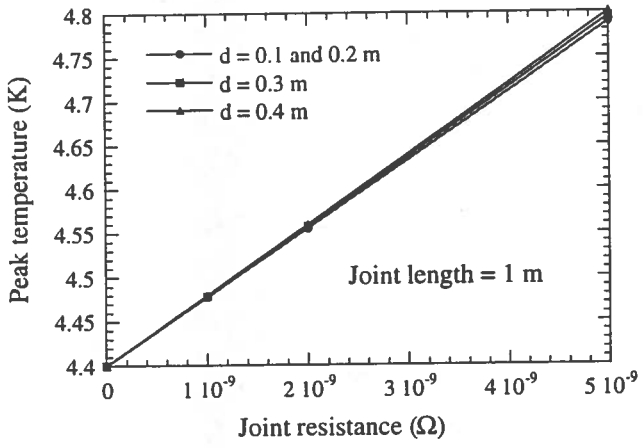

Fig. G2: Peak temperature as function of the joint resistance for various values of the distance between coolers and corresponding to a joint length of 1 m

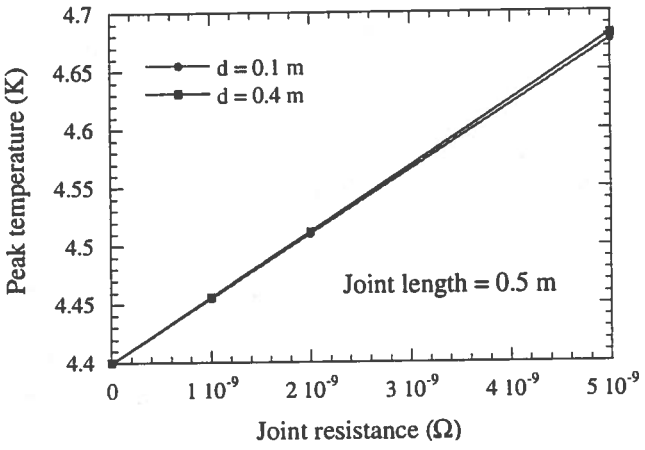

Fig. G3: Peak temperature as function of the joint resistance for various values of the distance between coolers and corresponding to a joint length of 0.5 m

In those conditions the peak temperature ranges from 4.5 to 4.8 K, depending on the joint resistance and length; 4.8 K should be taken as operative temperature.
The dependence of the peak temperature by the distance between coolers is negligible.
In Figs. G4 and G5 the number of conductor in the transverse direction at T>4.4 K as function of the joint resistance, for various values of the distance between coolers and for a joint length of respectively 1 m and 0.5 m is shown.

The maximum number of heated conductor is 21, corresponding to a joint resistance of $5 \cdot 10^{-9}$ Ω and a joint length of 1 m; in order to avoid that the joints could interact one each others, and since the length of one turn is about 20 m, the minimum length between two joints should be about 20·21 = 420 m.

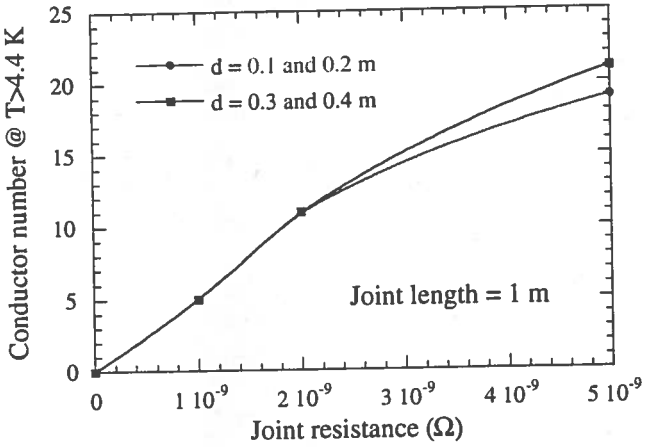

Fig. G4: Transverse length corresponding to a temperature T>4.4 K as function of the joint resistance for various values of the distance between coolers (joint length = 1 m)

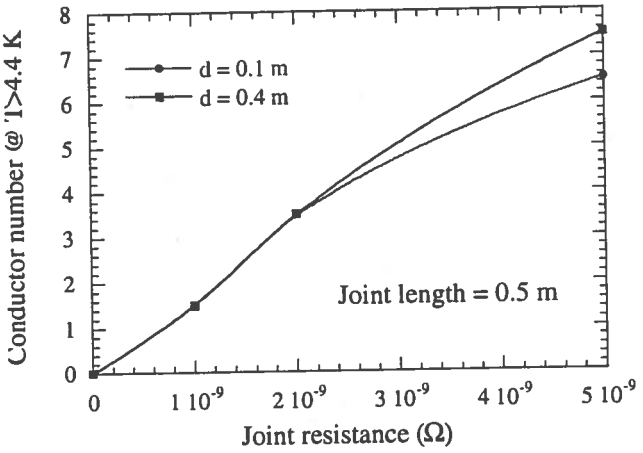

Fig. G5: Transverse length corresponding to a temperature T>4.4 K as function of the joint resistance for various values of the distance between coolers (joint length = 0.5 m)

In Figs. G6 and G7 the longitudinal length corresponding to a temperature T>4.4 K as function of the joint resistance, for various values of the distance between coolers and for a joint length of respectively 1 m and 0.5 m is shown.
In the worst case the heat propagates up to 8 m, which means about 2/5 of one turn.
In this case the dependence by the distance between the coolers is more significative.

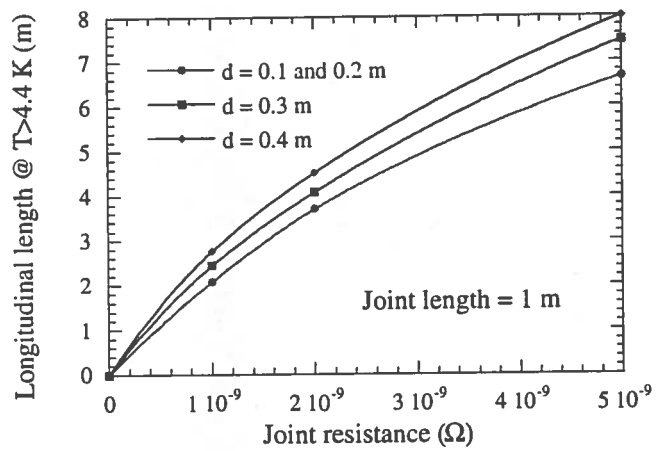

Fig. G6: Longitudinal length corresponding to a temperature T>4.4 K as function of the joint resistance for various values of the distance between coolers (joint length = 1 m)

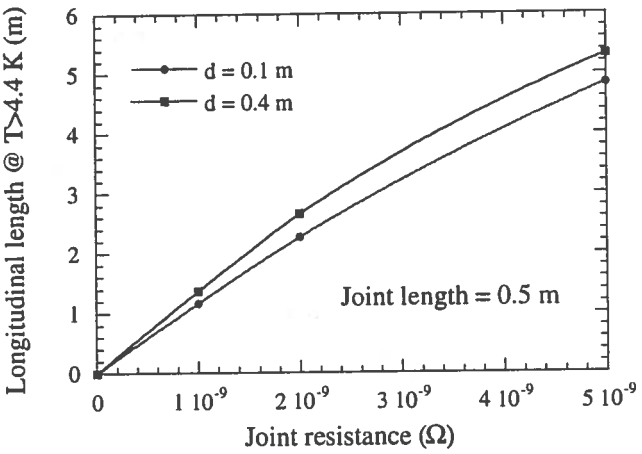

Fig. G7: Longitudinal length corresponding to a temperature T>4.4 K as function of the joint resistance for various values of the distance between coolers (joint length = 0.5 m)

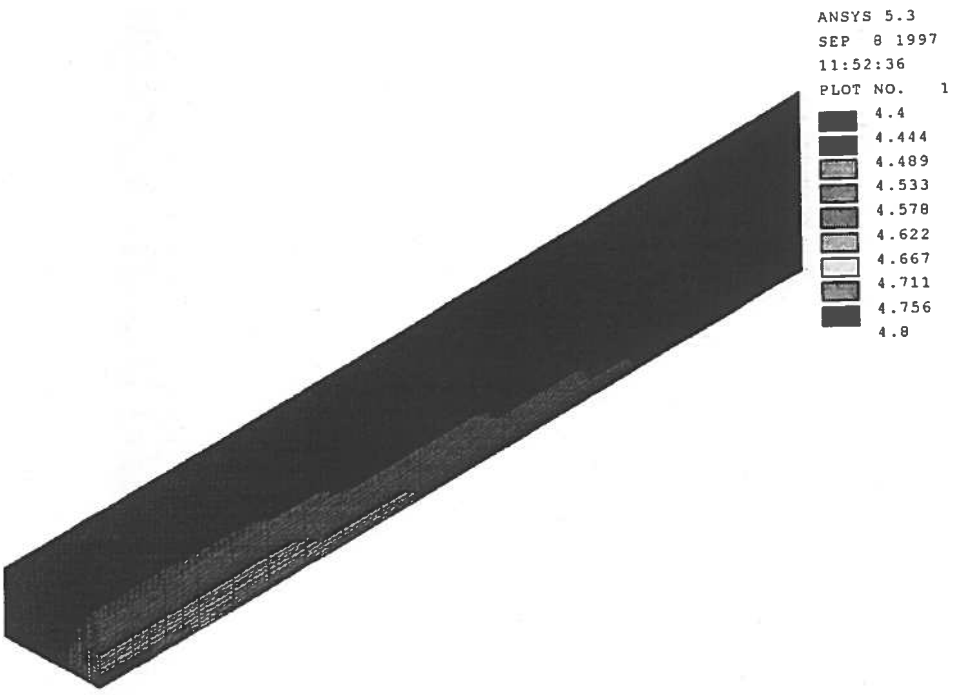

Fig. G8: Temperature distribution in the case $5 \cdot 10^{-9}$ Ω joint resistance, 1 m joint length and 0.4 m distance between heat exchangers

APPENDIX H

COMPARISON BETWEEN MONOLITHIC AND 5 MODULES CONFIGURATION FOR CMS WINDING

November 27, 1997

1 INTRODUCTION

The aim of this paper is to study a modular CMS winding configuration and to compare it to the monolithic design presented in the Technical Design Report (CERN/LHCC 97-10 CMS TDR1). There are three main characteristics that completely define the monolithic design:

- the conductor configuration
- the mechanical structure
- the layer numbers

The CMS conductor configuration has been widely studied during last years (see Appendix E), leading to the choice of the "block" conductor as best solution, since in that configuration the pure aluminium is not a *structural* material (see Fig. H1). Then no further studies on the conductor configuration are needed.

Table H.I: Main parameters of the monolithic design and some alternative solutions

	MONOLITHIC DESIGN (4 layers)	4 MODULES DESIGN (5 layers)	4 MODULES DESIGN (4 layers)	**5 MODULES DESIGN (4 layers)**
Strand number	**36**	26	36	**36**
Conductor dimensions (bare) (mm×mm)	**72×22.3**	50.88×20	63.52×22	**63.8×22**
Operative current (A)	**19500**	14190	19500	**19572**
Number of turns/layer	**542**	596	542	**540**
Total number of turns	**2168**	2980	2168	**2160**
Inductance (H)	**14**	26	14	**14**
Outer cylinder thickness (mm)	**12**	50	50	**50**
Flange thickness (mm)	**-----**	25	25	**25**
1 module length (m)	**12.40**	3.11	3.11	**2.49**
Total length (m)	**12.40**	12.46	12.43	**12.44**
Winding thickness (mm)	**305.**	310.4	309.1	**310.2**
Average conductor length of 1 layer (Km)	**11.3**	3.1	2.8	**2.25**
Conductor length of 1 module (Km)	**45.3**	15.5	11.3	**8.98**
Required unit length (Km)	**11.3 or 5.65 or 2.825**	3.1	2.8	**2.25**
Total conductor length (Km)	**45.3**	62.0	45.1	**44.9**

The mechanical structure of CMS winding is different from all other existing thin solenoids: according to the monolithic design, the magnet is completely self-supported, the reinforcement being in the conductor itself. The absence of a modular structure (as in T.P.), i.e. the choice to wind only one module, has the advantage to optimise the stress in the insulation, minimising the number of perturbative factors in the winding, such as flanges or junctions. Anyway this solution could be risky, in the sense that whatever failure could happen, could lead to a complete failure of the winding. So it is interesting to study a modular design as much as possible *equivalent* to the monolithic one. Since in the monolithic design the critical region, from the point of view of stresses in the insulation, is the coil centre, the choice was to study a "five module solution". In this way no flanges lay in the central region, reproducing the behaviour of the monolithic winding.
According to studies made at CEA, CERN, INFN and ANSALDO, the layer number in the monolithic design is fixed to four. The possibility to wind five layers has been taken into account, but due to several difficulties on the electrical coupling between modules, it has been preferred to study as alternative solution a four layers modular structure.
This alternative design has been dimensioned trying to keep as constant the amount of materials involved in the design and the overall dimensions of the winding. In Table H.I the main parameters of the monolithic design and some alternative solutions are shown.

2 THE MODELS

The monolithic winding is a complete self supported structure, in which the outer cylinder (12 mm thick) has only an electrical function. In a modular structure this is not possible: in order to couple the modules the outer cylinder should have also a mechanical function. So that, choosing a 50 mm thick cylinder, the conductor has to be re-dimensioned in order to keep as constant the total amount of Al alloy in the winding. The pure Al dimensions and the number of turns also have been slightly modified in order to keep as constant the overall dimensions of the winding. In Fig. H1 a scale drawing of the two configurations is shown.
In Fig. H2 a scale drawing of the flange region of the modular design is shown. Each flange is constituted of a false turn, carrying no current (red cables), and a thin layer of fibre glass epoxy (~3 mm).

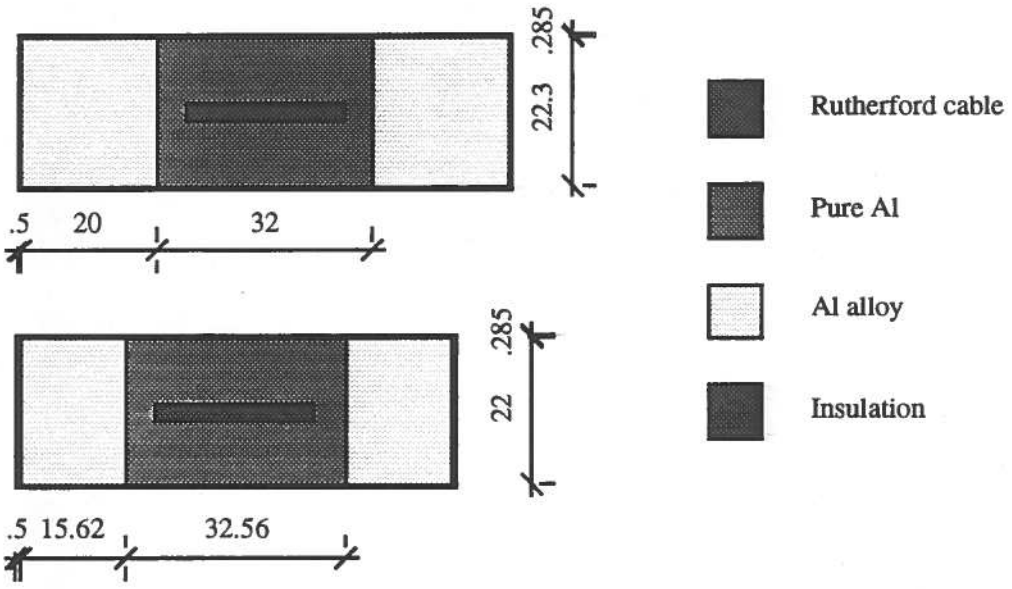

Fig. H1: Monolithic (upper) and modular (lower) design conductor (to scale)

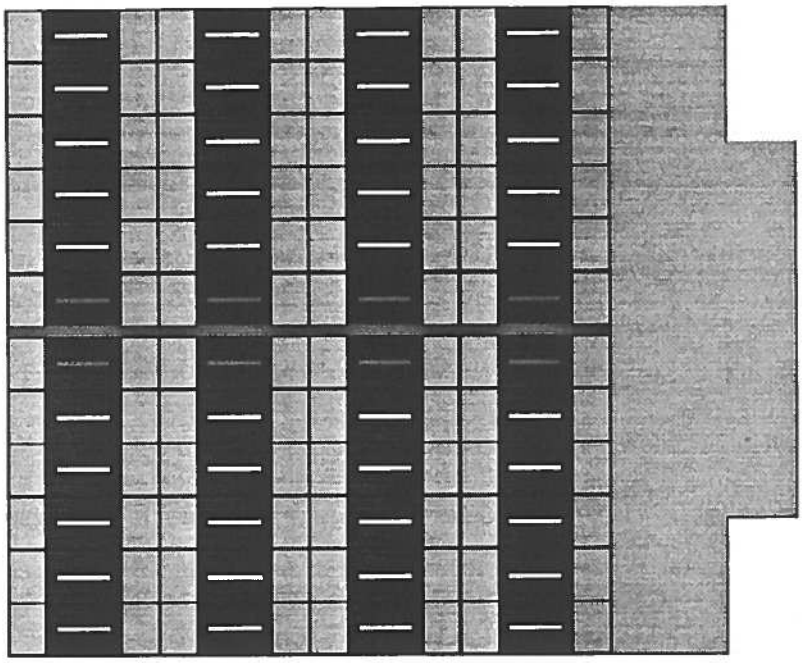

Fig. H2: Modular design flange region (to scale)

3 MATERIAL PROPERTIES

In Table H.II the material properties used in FE calculations are shown; the stress strain curve of pure Al represents as usual a pure aluminium annealed at 420 K (yield at 10÷15 MPa).

Table H.II: Material properties used in FE calculations

Material	Young's modulus [GPa]	Mean integral thermal expansion coefficient [K^{-1}]	Poisson ratio
Pure Al	σ–ε curve	$14.23 \cdot 10^{-6}$	0.33
Al alloy 6061	86.	$14.16 \cdot 10^{-6}$	0.33
SC strand	90.	$8.79 \cdot 10^{-6}$	0.33
Fibre glass epoxy in the plane of the ribbon	23.	$10.38 \cdot 10^{-6}$	0.37
Fibre glass epoxy $\perp$ to the plane of the ribbon	15.	$20.77 \cdot 10^{-6}$	0.37

4 THE RESULTS

The FE stress analysis has been carried out for the two usual operating conditions:

- Coil at 4.5 K
- Coil at 4.5 K, energised

Two locations have been studied into detail for each design. For the monolithic design coil centre and coil ends are the more critical regions of the winding. For the modular design the behaviour of the monolithic one should be reproduced in the coil centre, whilst the most critical region should be the flanges nearest to the coil centre.

4.1 Von Mises stress in conductor's components

In Tables H.III to H.VI the maximum Von Mises stress in conductor's components and the maximum Von Mises and shear stress at interfaces are shown for the monolithic design and the modular design.
There is a general agreement between results; this is because the stress on pure Al and Al alloy does not depend on the winding configuration, but on the ratio of pure Al and Al alloy areas, which has been kept as constant. The stresses in those materials are well under the allowable values.

Table H.III: Monolithic design - Maximum Von Mises stress in conductor's components

Material	Von Mises stress (MPa) Coil centre	Von Mises stress (MPa) Coil end
Coil at 4.5 K		
Pure Aluminium	4→18	5→19
SC Cable	138→164	138→165
Al Alloy	0→20	0→23
Coil at 4.5 K, energised		
Pure Aluminium	15→23	13→21
SC Cable	31→105	62→114
Al Alloy	113→129	68→82

Table H.IV: Modular design - Maximum Von Mises stress in conductor's components

Material	Von Mises stress (MPa) Coil centre	Von Mises stress (MPa) Flange nearest to coil centre
Coil at 4.5 K		
Pure Aluminium	8→18	4→18
SC Cable	138→161	138→163
Al Alloy	0→15	0→23
Coil at 4.5 K, energised		
Pure Aluminium	16→20	15→21
SC Cable	19→76	25→83
Al Alloy	130→146	115→142

Table H.V: Monolithic design - Maximum Von Mises and shear stress at interfaces (Al side)

Material bonding	Max. Von Mises stress (MPa)		Max. shear stress (MPa)	
Coil at 4.5 K				
	Coil centre	Coil end	Coil centre	Coil end
SC Cable÷Pure Al	14→20	14→20	11	11
Pure Al÷Al alloy	6→16	5→16	9	9
Coil at 4.5 K, energised				
	Coil centre	Coil end	Coil centre	Coil end
SC Cable÷Pure Al	16→22	15→21	11	11
Pure Al÷Al alloy	15→19	14→18	9	9

Table H.VI: Modular design - Maximum Von Mises and shear stress at interfaces (Al side)

Material bonding	Max. Von Mises stress (MPa)		Max. shear stress (MPa)	
Coil at 4.5 K				
	Coil centre	Flange nearest to coil centre	Coil centre	Flange nearest to coil centre
SC Cable÷Pure Al	14→20	14→19	11	10
Pure Al÷Al alloy	8→14	3→15	9	8
Coil at 4.5 K, energised				
	Coil centre	Flange nearest to coil centre	Coil centre	Flange nearest to coil centre
SC Cable÷Pure Al	17→21	17→21	9	9
Pure Al÷Al alloy	16→17	16→18	6	7

4.2 Stress in the insulation

Since the monolithic winding has been designed to optimise the stresses in the insulation, the only critical point of any modular design is just the behaviour of the insulation. The results will be compared adopting the Mohr-Coulomb criterion: in the plane σ_{mean} - τ_{max}, the stress status of each node in the insulation will be shown, together with the two Mohr circles corresponding to the maximum stress at zero shear and to the maximum shear at zero stress. That gives an idea of the failure envelope of the insulation under working conditions.
In Fig. H.3 to H.10 the Mohr-Coulomb plots of the insulation in the monolithic and modular design in the two considered locations and in the two operating conditions are shown.
Consider first the coil at 4.5 K (Fig. H.3-4 and Fig. H.7-8). Under this operating condition the two designs behave nearly in the same way, the coil centre of the monolithic design being the worst situation from all the points of view, maximum shear (23 MPa), maximum tensile and compressive stress (17 and -67 MPa respectively).
The condition of the coil at 4.5 K, energised is different (Fig. H.5-6 and Fig. H.9-10).
In the monolithic design, the cool down gives the largest contribution to the stress status of the insulation; the magnetic forces only contribute to spread out the stress distribution. The maximum stress values found are:

- Maximum shear: 23 MPa (coil centre)
- Maximum tensile stress: 13 MPa (coil centre)
- Maximum compressive stress: -56 MPa (coil end).

In the modular design, even if the maximum stress values are not really higher than in the monolithic one (26.5 MPa maximum shear, 16 and -67 MPa maximum tensile and compressive stress respectively), the distribution of the node stress status is larger and split into three regions:

- The point concentration region on the right represents the insulation perpendicular to magnet axis and adjacent to pure Al in the conductor. This part of insulation has the same stress status in the two designs, due to the fact that the stress conditions of pure Al do not change from the monolithic to the modular design.
- The upper concentration region represents the insulation parallel to magnet axis. This part of insulation greatly contributes to increase the maximum values of tensile and shear stress in the

region of the flange nearest to coil centre. This is due to the increased thickness of Al alloy outer cylinder, from 12 to 50 mm; actually the maximum values of shear can be found in the insulation adjacent to the cylinder and near to the flanges.

- Finally the points concentration region on the left represents the insulation perpendicular to magnet axis and adjacent to Al alloy in the conductor. This part of insulation contributes with the maximum values of compressive stress, which, anyway, remain comparable to the ones obtained with the monolithic design.

The conclusion is that the only critical region is the insulation which connects the winding to the outer cylinder, and more generally the insulation parallel to magnet axis near the flanges. The optimisation of the modular design comes down to the maximum allowable improvement of the stress status of that insulation.

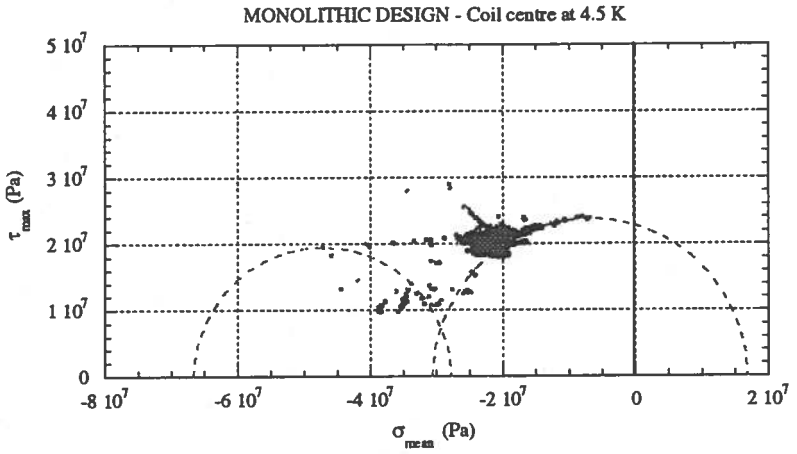

Fig. H3: Monolithic design - Mohr plot of the insulation in the coil centre at 4.5 K

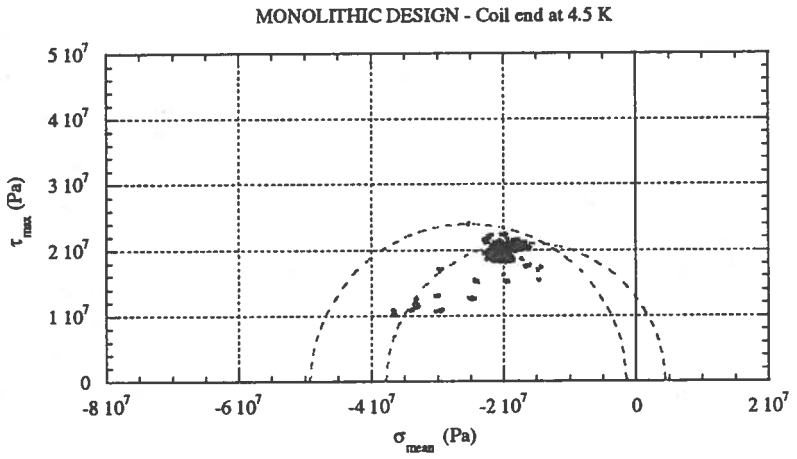

Fig. H4: Monolithic design - Mohr plot of the insulation in the coil end at 4.5 K

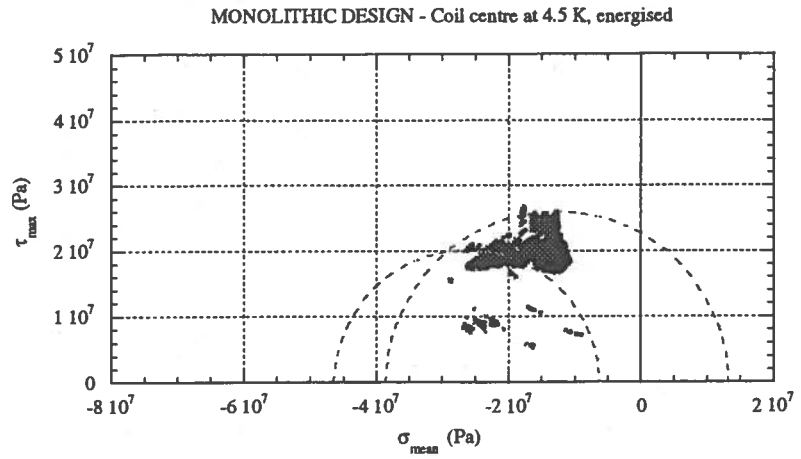

Fig. H5: Monolithic design - Mohr plot of the insulation in the coil centre at 4.5 K, energised

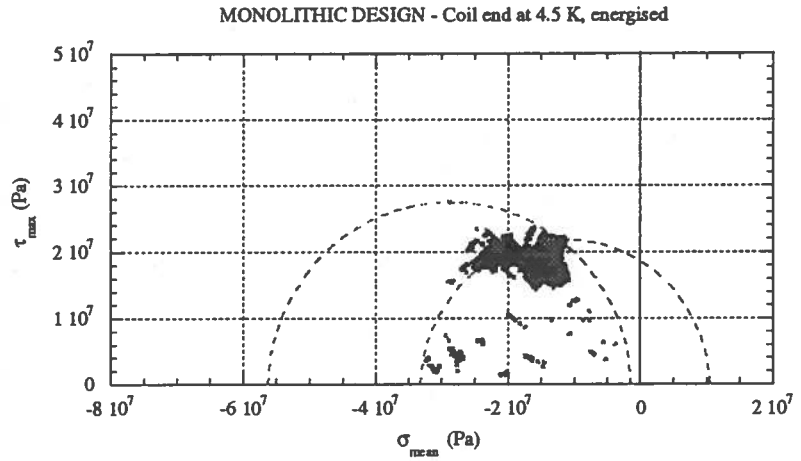

Fig. H6: Monolithic design - Mohr plot of the insulation in the coil end at 4.5 K, energised

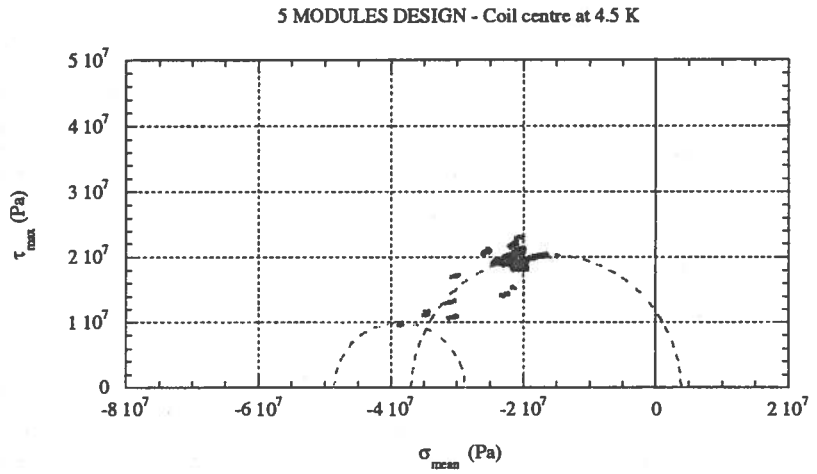

Fig. H7: Modular design - Mohr plot of the insulation in the coil centre at 4.5 K

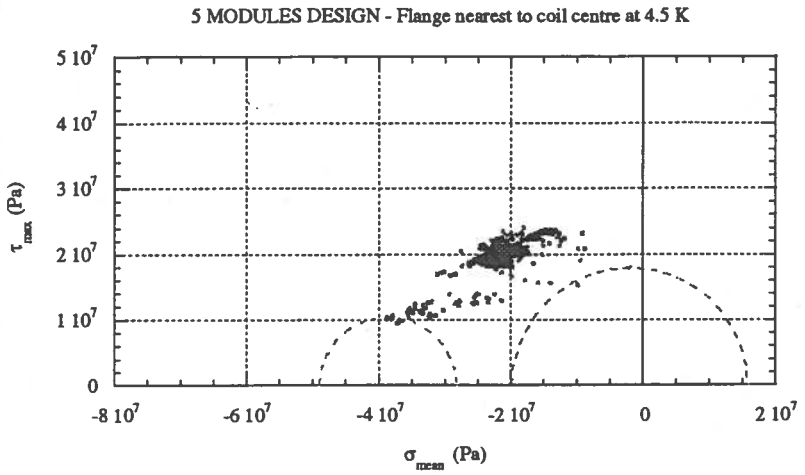

Fig. H8: Modular design - Mohr plot of the insulation in the flange nearest to coil centre at 4.5 K

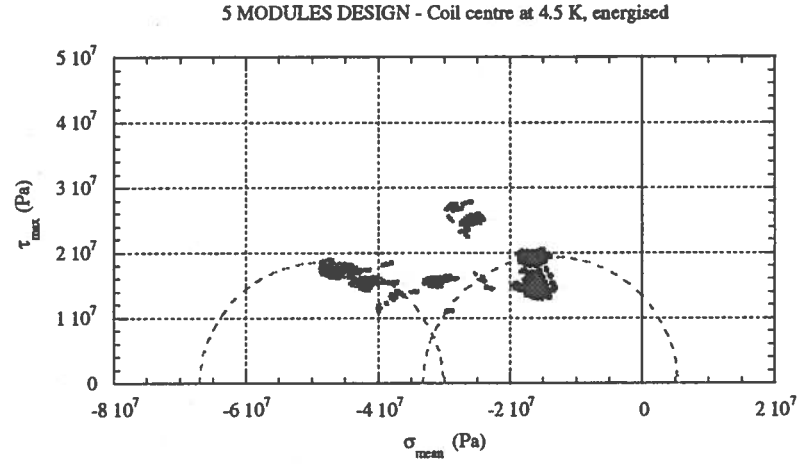

Fig. H9: Modular design - Mohr plot of the insulation in the coil centre at 4.5 K, energised

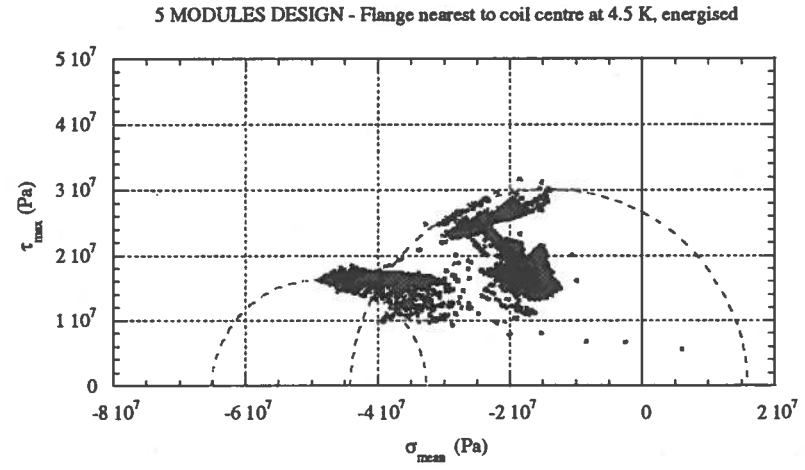

Fig. H10: Modular design - Mohr plot of the insulation in the flange nearest to coil centre at 4.5 K, energised

5 FINAL CONSIDERATIONS

The previous analysis is based on the first attempt made by designers to define the geometry of the 5 modules design for CMS winding. Several improvements have been made in order to compact as much as possible the structure. The result is a complex design (see Fig. H12) in which only one turn in each flange does not carry the current. Then a further simulation of the region near the flanges was needed to check the effects of this new configuration. The result is shown in Fig. H11; no main differences can be pointed out comparing this figure to Fig. H10, which shows the stress status of the insulation with all the false turns carrying no current. This means that the stress status of the insulation is completely determined by the geometry of the flanges.

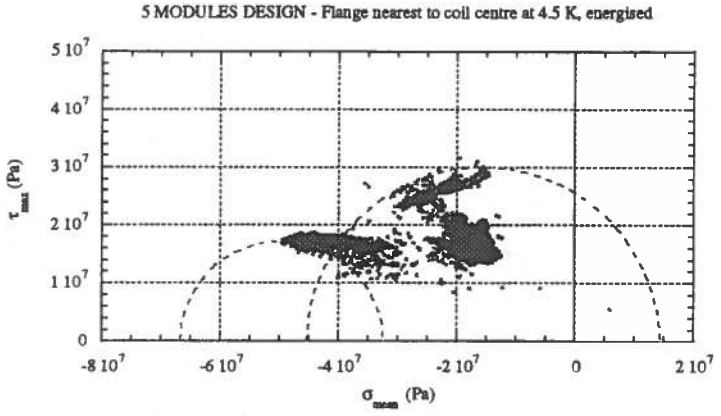

Fig. H11: Modular design with 3 turns of each flange carrying the current - Mohr plot of the insulation in the flange nearest to coil centre at 4.5 K, energised

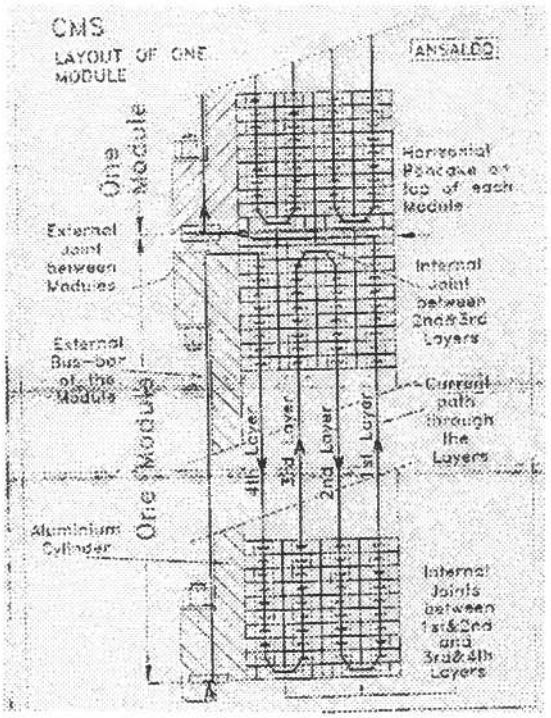

Fig. H12: Detail of coupling between modules